Author(s): Tedja, Milly S.; Wojciechowski, Robert; Hysi, Pirro G.; Eriksson, Nicholas; Furlotte, Nicholas A.; Verhoeven, Virginie J. M.; Iglesias, Adriana I.; Meester-Smoor, Magda A.; Tompson, Stuart W.; Fan, Qiao; Khawaja, Anthony P.; Cheng, Ching-Yu; Höhn, René; Yamashiro, Kenji; Wenocur, Adam; Grazal, Clare; Haller, Toomas; Metspalu, Andres; Wedenoja, Juho; Jonas, Jost B.; Wang, Ya Xing; Xie, Jing;

Title: Genome-wide association meta-analysis highlights light-induced signaling as a driver for refractive error

Year: 2018

Version: Accepted version (Final draft)

Please cite the original version:

Tedja, M. S., Wojciechowski, R., Hysi, P. G., Eriksson, N., Furlotte, N. A., Verhoeven, V. J. M., Iglesias, A. I., Meester-Smoor, M. A., Tompson, S. W., Fan, Q., Khawaja, A. P., Cheng, C.-Y., Höhn, R., Yamashiro, K., Wenocur, A., Grazal, C., Haller, T., Metspalu, A., Wedenoja, J., . . . Klaver, C. C. W. (2018). Genome-wide association meta-analysis highlights light-induced signaling as a driver for refractive error. Nature Genetics, 50(6), 834-848. https://doi.org/10.1038/s41588-018-0127-7

Large genome-wide meta-analysis highlights light-induced signaling as a driver for refractive error

Milly S. Tedja[1,2,76], Robert Wojciechowski[3,4,76], Pirro G. Hysi[5,76], Nicholas Eriksson[6,76], Nicholas A. Furlotte[6,76], Virginie J.M. Verhoeven[1,2,7,76], Stuart W.J. Tompson[8], Adriana I. Iglesias Gonzalez[2], Qiao Fan[9], Anthony P. Khawaja[10], Ching-Yu Cheng[9,11], René Höhn[12,13], Elisabeth M. van Leeuwen[1,2], Kenji Yamashiro[14], Adam Wenocur[15], Clare Grazal[15], Toomas Haller[16], Andres Metspalu[16], Juho Wedenoja[17,18], Jost B. Jonas[19,20], Ya Xing Wang[20], Jing Xie[21], Paul Mitchell[22], Paul J. Foster[23], Barbara E.K. Klein[8], Ronald Klein[8], Andrew D. Paterson[24], Mohsen S. Hosseini[24], Rupal L. Shah[25], Cathy Williams[26], Yik Ying Teo[27,28], Yih Chung Tham[11], Preeti Gupta[29], Wanting Zhao[30], Yuan Shi[30], Woei-Yuh Saw[31], E Shyong Tai[28], Xue Ling Sim[28], Jennifer E. Huffman[32], Ozren Polašek[33], Caroline Hayward[32], Goran Bencic[34], Igor Rudan[35], James F. Wilson[35], CREAM[#], 23andMe Research Team, Peter K. Joshi[35], Akitaka Tsujikawa[14], Fumihiko Matsuda[36], Kristina N. Whisenhunt[8], Tanja Zeller[37], Peter J. van der Spek[38], Roxanna Haak[38], Arthur A. B. Bergen[39,40], Hanne Meijers-Heijboer[40,41], Magda A. Meester-Smoor[1,2], Sudha K. Iyengar[42-44], Jonathan H. Lass[42,43], Albert Hofman[2,45,46], Fernando Rivadeneira[2,46,47], André G. Uitterlinden[2,46,47], Johannes R. Vingerling[1], Terho Lehtimäki[48,49], Olli T. Raitakari[50,51], Ginevra Biino[52], Maria Pina Concas[53], Tae Hwi Schwantes-An[4,54], Robert P. Igo, Jr.[42], Gabriel Cuellar[55], Nicholas G. Martin[56], Jamie E. Craig[57], Puya Gharahkhani[55], Katie M. Williams[5], Abhishek Nag[58], Jugnoo S. Rahi[59], Phillippa Cumberland[59], Cécile Delcourt[60], Céline Bellenguez[61-63], Janina S. Ried[64], Thomas Meitinger[65,66], Christian Gieger[64], Tien Yin Wong[67,68], Alex W. Hewitt[21,69], David A. Mackey[70], Claire L. Simpson[4,71], Norbert Pfeiffer[13], Olavi Pärssinen[72,73], Paul N. Baird[21], Veronique Vitart[32], Najaf Amin[2], Cornelia M. van Duijn[2], Joan E. Bailey-Wilson[4], Terri L. Young[8], Seang Mei Saw [28,74], Dwight Stambolian[15], Stuart MacGregor[55], Jeremy A. Guggenheim[25,77], Joyce Tung[6,77], Christopher J. Hammond[5,77], Caroline C.W. Klaver[1,2,75,77]

Affiliations

1. Department of Ophthalmology, Erasmus Medical Center, Rotterdam, The Netherlands.
2. Department of Epidemiology, Erasmus Medical Center, Rotterdam, The Netherlands.
3. Department of Epidemiology and Medicine, Johns Hopkins Bloomberg School of Public Health, Baltimore, Maryland, USA.
4. Computational and Statistical Genomics Branch, National Human Genome Research Institute, National Institutes of Health, Bethesda, Maryland, USA.
5. Department of Ophthalmology, King's College London, London, UK.
6. 23andMe, Inc., Mountain View, USA.
7. Department of Clinical Genetics, Erasmus Medical Center, Rotterdam, The Netherlands.
8. Department of Ophthalmology and Visual Sciences, University of Wisconsin School of Medicine and Public Health, Madison, Wisconsin, USA.
9. Ophthalmology & Visual Sciences Academic Clinical Program and Centre for Quantitative Medicine, DUKE-National University of Singapore, Singapore.
10. Department of Public Health and Primary Care, University of Cambridge, Cambridge, UK.
11. Ocular Epidemiology Research Group, Singapore Eye Research Institute, Singapore National Eye Centre, Singapore, Singapore.
12. Department of Ophthalmology, University Hospital Bern, Inselspital, University of Bern, Bern, Switzerland.
13. Department of Ophthalmology, University Medical Center Mainz, Mainz, Germany.
14. Department of Ophthalmology and Visual Sciences, Kyoto University Graduate School of Medicine, Kyoto, Japan.
15. Department of Ophthalmology, University of Pennsylvania, Philadelphia, Pennsylvania, USA.
16. Estonian Genome Center, University of Tartu, Tartu, Estonia.
17. Department of Ophthalmology, Helsinki University Hospital, University of Helsinki, Helsinki, Finland.
18. Department of Public Health, University of Helsinki, Helsinki, Finland.
19. Department of Ophthalmology, Medical Faculty Mannheim of the Ruprecht-Karls-University of Heidelberg, Mannheim, Germany.
20. Beijing Institute of Ophthalmology, Beijing Key Laboratory of Ophthalmology and Visual Sciences, Beijing Tongren Eye Center, Beijing Tongren Hospital, Capital Medical University, Beijing, China.
21. Centre for Eye Research Australia, University of Melbourne, Melbourne, Australia.
22. Department of Ophthalmology, Centre for Vision Research, Westmead Institute for Medical Research, University of Sydney, Sydney, Australia.
23. NIHR Biomedical Research Centre, Moorfields Eye Hospital NHS Foundation Trust and UCL Institute of Ophthalmology, London, UK.
24. Program in Genetics and Genome Biology, Hospital for Sick Children and University of Toronto, Toronto, Ontario, Canada.
25. School of Optometry & Vision Sciences, Cardiff University, Cardiff, UK.
26. School of Social and Community Medicine, University of Bristol, Bristol, UK.
27. Department of Statistics and Applied Probability, National University of Singapore, Singapore, Singapore.
28. Saw Swee Hock School of Public Health, National University Health Systems, National University of Singapore, Singapore, Singapore.
29. Department of Health Service Research, Singapore Eye Research Institute, Singapore National Eye Centre, Singapore, Singapore.
30. Statistics Support Platform, Singapore Eye Research Institute, Singapore National Eye Centre, Singapore, Singapore.
31. Life Sciences Institute, National University of Singapore, Singapore, Singapore.

32. Institute of Genetics and Molecular Medicine, Medical Research Council Human Genetics Unit, University of Edinburgh, Edinburgh, UK.
33. Faculty of Medicine, University of Split, Split, Croatia.
34. Department of Ophthalmology, Sisters of Mercy University Hospital, Zagreb, Croatia.
35. Centre for Global Health Research, Usher Institute for Population Health Sciences and Informatics, University of Edinburgh, Edinburgh, UK.
36. Center for Genomic Medicine, Kyoto University Graduate School of Medicine, Kyoto, Japan.
37. Clinic for General and Interventional Cardiology, University Heart Center Hamburg, Hamburg, Germany.
38. Department of Bioinformatics, Erasmus Medical Center, Rotterdam, The Netherlands.
39. Department of Ophthalmology, Academic Medical Center, Amsterdam, The Netherlands.
40. Department of Clinical Genetics, Academic Medical Center, Amsterdam, The Netherlands.
41. Department of Clinical Genetics, VU University Medical Center, Amsterdam, The Netherlands.
42. Department of Epidemiology and Biostatistics, Case Western Reserve University, Cleveland, Ohio, USA.
43. Department of Ophthalmology and Visual Sciences, Case Western Reserve University and University Hospitals Eye Institute, Cleveland, Ohio, USA.
44. Department of Genetics, Case Western Reserve University, Cleveland, Ohio, USA.
45. Department of Epidemiology, Harvard T.H. Chan School of Public Health, Boston, Massachusetts, USA.
46. Netherlands Consortium for Healthy Ageing, Netherlands Genomics Initiative, the Hague, the Netherlands.
47. Department of Internal Medicine, Erasmus Medical Center, Rotterdam, The Netherlands.
48. Department of Clinical Chemistry, University of Tampere School of Medicine, Tampere, Finland.
49. Department of Clinical Chemistry, Fimlab Laboratories, University of Tampere, Tampere, Finland.
50. Research Centre of Applied and Preventive Cardiovascular Medicine, University of Turku, Turku, Finland.
51. Department of Clinical Physiology and Nuclear Medicine, Turku University Hospital, Turku, Finland.
52. Institute of Molecular Genetics, National Research Council of Italy, Sassari, Italy.
53. Institute of Genetic and Biomedical Research, National Research Council of Italy, Sassari, Italy.
54. Department of Medical and Molecular Genetics, Indiana University - Purdue University Indianapolis, Indianapolis, Indiana, USA.
55. Department of Statistical Genetics, Queensland Institute of Medical Research, Brisbane, Australia.
56. Department of Genetic Epidemiology, Queensland Institute of Medical Research, Brisbane, Australia.
57. Department of Ophthalmology, Flinders University, Adelaide, Australia.
58. Department of Twin Research and Genetic Epidemiology, King's College London, London, UK.
59. Great Ormond Street Institute of Child Health, University College London, London, UK.
60. Team LEHA, UMR 1219, Université de Bordeaux, Inserm, Bordeaux Population Health Research Center, Bordeaux, France.
61. Institut Pasteur de Lille, Lille, France.
62. Université de Lille, U1167, Lille, France.
63. Inserm, U1167, Lille, France.
64. Institute of Genetic Epidemiology, Helmholtz Zentrum München—German Research Center for Environmental Health, Neuherberg, Germany.
65. Institute of Human Genetics, Helmholtz Zentrum München, Neuherberg, Germany.
66. Institute of Human Genetics, Klinikum rechts der Isar, Technische Universität München, Munich, Germany.

67. Academic Medicine Research Institute, Singapore.
68. Retino Center, Singapore National Eye Centre, Singapore, Singapore.
69. Department of Ophthalmology, Menzies Institute of Medical Research, University of Tasmania, Hobart, Australia.
70. Centre for Ophthalmology and Visual Science, Lions Eye Institute, University of Western Australia, Perth, Australia.
71. Department of Genetics, Genomics and Informatics, University of Tennessee Health Sciences Center, Memphis, Tenessee.
72. Department of Ophthalmology, Central Hospital of Central Finland, Jyväskylä, Finland.
73. Gerontology Research Center and Department of Health Sciences, University of Jyväskylä, Jyväskylä, Finland.
74. Myopia Research Group, Singapore Eye Research Institute, Singapore National Eye Centre, Singapore, Singapore.
75. Department of Ophthalmology, Radboud University Medical Center, Nijmegen, The Netherlands.
76. These authors contributed equally to this work.
77. These authors jointly directed this work.

A full list of consortium members appears at the end of the paper.

Corresponding author

Prof. dr. Caroline C.W. Klaver, Erasmus Medical Center, room Na-2808, PO Box 2040, 3000 CA, Rotterdam, the Netherlands, e-mail: c.c.w.klaver@erasmusmc.nl, phone number +31651934491, fax number +31107044657

Abstract

Refractive errors, including myopia, are the most frequent eye disorders worldwide and an increasingly common cause of blindness. Through a genome-wide association meta-analysis in 160,420 participants of mixed ancestry from CREAM and 23andMe and replication in 95,505 participants from the UK Biobank, we increased the number of significant independent signals from 37 to 161 and found a high genetic correlation between Europeans and Asians (>0.78). Enrichment analysis identified retinal cell physiology and light processing as the most prominent mechanisms. Expression experiments and comprehensive *in silico* analyses of the novel genes showed functional contribution of all cell types in the neurosensory retina (*GNB3, DRD1, AKAP6, ZEB2, TFAP2B, CA8, EDN2*), the retinal pigment epithelium (*EFEMP1, ANO2*), vascular endothelium (*CD34, FLT1*), and extracellular matrix (*VIPR2, ANTXR2, TCF7L2, COL10A1*) to refractive error development. The newly identified genes also elicited novel mechanisms such as rod as well as cone bipolar synaptic neurotransmission (rod: *CLU*; cone: *GNB3*), anterior segment morphology (*TCF7L2, VIPR2, MAF*), and angiogenesis (*FLT1*). Twenty eight SNPs resided in or near DNA structures transcribing small RNAs (non-coding, tRNAs, snoRNas, rRNAs, miRNA), suggesting a role for post-transcriptional regulation. Our results support the notion that refractive errors are caused by a light-dependent retina-to-sclera signaling cascade, and delineate potential molecular drivers defining the pathobiology of refractive errors and myopia.

Introduction

Refractive errors are common optical aberrations determined by mismatches in the focusing power of the cornea, lens and axial length of the eye. Their distribution is rapidly shifting towards myopia, or nearsightedness, all over the world. The myopia boom is particularly prominent in urban East Asia where up to 95% of twenty-year-olds in cities such as Seoul and Singapore have this refractive error[1-4]. Myopia prevalence is also rising throughout Western Europe and the USA, affecting ~50% of young adults in these regions[5,6]. While refractive errors can be optically corrected, even at moderate values they carry a significant risk of ocular complications with a high economic burden[7-9]. One in three individuals with high myopia (-6 diopters or worse) will develop irreversible visual impairment or blindness, mostly due to myopic macular degeneration, retinal detachment, or glaucoma[10,11]. At the other extreme, high hyperopia predisposes to strabismus, amblyopia and angle-closure glaucoma[10,12].

Refractive errors result from a complex interplay of lifestyle and genetic factors. Most established lifestyle factors for myopia are high education, lack of outdoor exposure, and excessive near work[3]. Recent research has identified many genetic variants for refractive errors, myopia, and axial length[13-25]. Two large studies, the international Consortium for Refractive Error and Myopia (CREAM)[26] and the personal genomics company 23andMe, Inc.[17,27] have provided the most comprehensive results. Despite differences in design and methodology, 37 associated genetic loci were identified in common, and most strikingly, there was a near-linear relationship in genetic effect sizes of the associated variants[28].

Given that only 3.6% of the variance of the refractive error trait was explained by the identified genetic variants[26], we presumed a high missing heritability. We therefore combined CREAM and 23andMe, and expanded the study sample to 160,420 individuals from a mixed ancestry population with quantitative information on refraction for a genome-wide association (GWA) meta-analysis. Significant variants were tested for replication in an independent cohort consisting of 95,505 individuals from the UK Biobank. We conducted systematic comparisons to assess differences in genetic inheritance and

distribution of risk variants between Europeans and Asians. Polygenic risk analyses were performed to evaluate the contribution of the identified variants to the risk of myopia and hyperopia. Finally, we integrated expression data and bioinformatics on the identified genes to gain insight into the possible mechanisms underlying the genetic associations.

RESULTS

Susceptibility loci for refractive error

We performed a GWAS meta-analysis on adult refractive error using summary statistics from 37 studies from the Consortium for Refractive Error and Myopia (CREAM) and two cohorts from the personal genomics company 23andMe (Supplementary Figure 1). Analyses were based on ~11 million genetic variants (SNPs, insertions and deletions) genotyped or imputed to 1000 Genomes Project Phase I reference panel (version 3, March 2012 release[29]) that passed extensive quality control (Supplementary Figures 2-5, Supplementary Table 1a) and were represented by at least half of the entire study population and by > 13 cohorts from CREAM and both cohorts from 23andMe.

Meta-analyses were conducted in three stages. *Stage 1* focused on CREAM and included a fixed effects inverse variance-weighted meta-analysis on 44,192 individuals of European descent (CREAM-EUR) and 11,935 participants of East or South Asian ancestry (CREAM-ASN) using untransformed spherical equivalent (SphE) as the dependent variable representing refractive error (Supplementary Table 1b). 1,063 variants clustering in 24 loci (Supplementary Excel File 1) were genome-wide significant (P 5 x 10^{-8}). *Stage 2* consisted of a fixed effects inversed variance-weighted meta-analysis of the two European 23andMe cohorts ($N_{23andMe\_V2}$= 12,128; $N_{23andMe\_V3}$ = 92,165) using age of diagnosis of myopia (AODM) as outcome[27]. A total of 5,205 genome-wide significant variants clustered in 112 loci (Supplementary Excel File 1). All 25 loci identified at Stage 1 replicated in Stage 2 (*pBonferroni* 2.00 x 10^{-3}). Vice versa, 29 (26%) of the loci identified at Stage 2 replicated in Stage 1 (*pBonferroni* 4.46 x 10^{-4}), an expected proportion given the lower statistical power in CREAM. *Stage 3* was the joint meta-analysis of Stage 1 and Stage 2. As CREAM and 23andMe applied different phenotype measures, we used signed Z-scores as the mean per-allele effect size and assigned equal weights to CREAM and 23andMe. We identified 7,967 genome-wide significant genetic variants clustering in 140 loci (Figure 1a; Supplementary Figure 5-6,

Supplementary Excel File 1 – 3, Supplementary PDF File 1 and 2) of which 104 were novel. All 37 loci that were found previously by CREAM and 23andMe using genotype data imputed to the HapMap II reference panel were replicated (*pBonferroni* 1.85 x 10^{-3}), and 36 of the 37 were genome-wide significant (Supplementary Table 2)[26,27]. We applied genomic control at each stage and checked for population stratification using LD score regression[30] (Supplementary Table 3). At Stage 1 and 2, population stratification was unlikely as inflation factors (λGC) were < 1.1 (Supplementary Figure 7), and LD score regression intercepts ($LDSC_{intercept}$) ranged from 0.892 to 1.023 (Supplementary Figure 8). At Stage 3, we observed an inflation of the median test statistic (λGC=1.129; Supplementary Figure 6), probably due to true polygenicity rather than bias (i.e. population stratification or cryptic relatedness)[31]. The mixed ancestry did not allow for calculation of $LDSC_{intercept}$.

To detect the presence of multiple independent signals at the discovered loci, a stepwise conditional analysis was performed with GCTA-COJO[32] on meta-analysis summary statistics from all European cohorts (*N*=148,485*)* using the Rotterdam Study I-III (RS I-III) as a reference panel for LD structure ($N_{RSI-III}$ = 10,775). This analysis yielded 27 additional independent variants, resulting in a total of 167 loci (Supplementary Excel File 1). The lead variants at the newly-discovered loci were mainly of lower minor allele frequencies (MAFs) than those reported in previous refractive error GWAS studies with lower samples, reflecting the increased statistical power of the current analysis (Figure 1b).

We advanced these loci for replication analysis in a GWAS of refractive error carried out by the UK Eye & Vision (UKEV) Consortium in 95,505 participants of European ancestry from the UK BioBank. [33]16 variants were not present in UKEV, and were represented by a surrogate variant in high LD (r^2 >0.8 LD; Supplementary Excel File 1). Six out of the 167 variants were not considered for replication analysis: one variant (rs188159083) was not present on the array nor a surrogate was available in UKEV and five variants showed evidence of departure from HWE (HWE exact test P < 3.0 x 10^{-4}, where 3.0 x 10^{-4} =0.05/167). One of these five variants (rs3138141, *RDH5*) was identified previously and therefore still considered as a refractive error risk variant[26,27]. The remaining 161 genetic variants were tested for replication. 86% (138/161) of the candidate variants replicated significantly: 104 (65%)

replicated surpassing genome wide significance; 34 replicated surpassing Bonferroni correction ($P < 3.0 \times 10^{-4}$; 21.1%); and, 12 showed nominal evidence for replication ($0.05 < P < 3.0 \times 10^{-4}$; 7.5%). Of the total, only 11 (7%) did not replicate (Table 1 and Supplementary Excel File 1).

As CREAM and 23andMe employed different phenotypic outcomes, we evaluated consistency of genotypic effects by comparing marker-wise additive genetic effect sizes (in units diopters per copy of the risk allele) for SphE from CREAM-EUR against those (in units log(HR) per copy of the risk allele) for AODM from 23andMe. All variants strongly associated with either outcome ($P < 0.001$), were concordant in direction-of-effect, and had highly correlated effect sizes (Figure 2 a,b; Supplementary Figure 9). For these variants, a 10% decrease in the log(HR) for AODM, indicating an earlier age-at-myopia onset, was associated with a decrease of 0.15 diopters in SphE. A quantitative analysis for all common SNPs (MAF > 0.01; HapMap3) using LD score regression yielded a genetic correlation of 0.93 (95% CI 0.86 to 0.99; $P = 2.1 \times 10^{-159}$), confirming that effect sizes for both phenotypic outcomes were closely related.

Gene annotation of susceptibility loci

We annotated all genetic variants with wANNOVAR using the University of California Santa Cruz (UCSC) Known Gene database[34,35]. The identified 139 genetic loci were annotated to 208 genetic structures (i.e. genes and known transcribed RNA genes, Table 1, Supplementary Excel file 1, Online Methods). The physical positions of the lead genetic variants relative to protein-coding genes are shown in Figure 1c. 86% of the identified variants were either intragenic or less than 50 kb from the 5'or 3' end of the transcription start site. We found seven exonic variants (Supplementary Table 4) of which two had MAF ≤ 0.05: rs5442 (*GNB3*) and rs17400325 (*PDE11A).* The index SNP in the *GNB3* locus with MAF 0.05 in Europeans is a highly conserved missense variant (G272S) predicted to be damaging by PolyPhen-2[36] and SIFT[37]. *PDE11A* is presumed to play a role in tumorigenesis, brain function, and inflammation[38]. The index SNP in the *PDE11A* locus with MAF 0.03 in Europeans is also a highly

conserved missense variant (Y727C); this variant was predicted to be damaging by PolyPhen[36], SIFT[39] and align GVGD[40,41].The other exonic variants, rs1064583 (*COL10A1*), rs807037 (*KAZALD1*), rs1550094 (*PRSS56*), rs35337422 (*RD3L*) and rs6420484 (*TSPAN10*), were not predicted to be damaging.

The most significant variant (Stage 3; rs12193446, $P = 4.21 \times 10^{-84}$) resides on chromosome 6 within a non-coding RNA, *BC035400*, in an intron of the *LAMA2* gene. This locus had been identified previously, but our current fine mapping redefined the most associated variant. The function and potential downstream target sites for BC035400 are currently unknown. The previously most strongly associated variant, rs524952 on chromosome 15 near *GJD2*, was the second most significant variant ($P = 2.28 \times 10^{-65}$).

Post-GWAS analyses identify 22 additional novel candidate loci

We performed two gene-based tests, fastBAT[42] and EUGENE[43], and applied a functional enrichment approach using fgwas[44] (Online Methods). Fgwas incorporates functional annotation (eg. DNase I hypersensitive sites in various tissues and 3'UTR regions) to reweight data from GWAS, and uses a Bayesian model to calculate a posterior probability of association. With fastBAT, we identified 13 genes at P value $< 2.0 \times 10^{-6}$, one of which (*CHD7*) had been identified previously[26,27]. Using EUGENE, we found 7 genes at P value $< 2.0 \times 10^{-6}$ after incorporation of blood eQTLs. With fgwas, we identified 6 loci, which could be annotated to 9 genes, at posterior probability >0.9. Two genes (*HMGN4* and *TLX1*) showed significant associations in two or more approaches. Taken together, these post-GWAS approaches resulted in a total of 22 additional candidate loci for refractive error, annotated to 25 genes (Supplementary Table 5). This increases the overall number of significant genetic associations to 161 candidate loci.

Polygenic risk scores

We calculated polygenic risk scores (PGRS)[45] per individual at various *P* value thresholds (Online Methods) for Rotterdam Study I-III (RS I-III; *N*=10,792) after recalculating *P* values and Z-scores of variants from Stage 3 excluding RS I-III. We found the highest fraction of phenotypic variance (7.8%) explained with 7,307 variants at *P* value threshold 0.005 (Supplementary Table 6). A PGRS based on these variants distinguished well between individuals with hyperopia and myopia at the lower and higher deciles (Figure 3); those in the highest decile had a 40-fold increased risk of myopia. When the PGRS was stratified for the median age (< 63 or > 63+ yrs), we found a significant difference in the variance explained (<63 yrs 8.9%; 63+ yrs 7.4%; *P* value 0.0038). The variance explained by PGRS was not significantly different between males and females (8.3% vs 7.5%; *P* value 0.13). The predictive value (area under the receiver operating characteristic curve, AUC) of the PGRS for myopia versus hyperopia adjusted for age and gender was 0.77 (95% CI = 0.75–0.79), a 10% increase compared to previous estimations[46].

Trans-ethnic comparison of genotypic effects

To explore potential ancestry differences in the identified refractive error loci, we calculated the heritability explained by common genetic variants (SNP-h^2) for Europeans and Asians using LD score regression[47]. SNP-h^2 was 0.214 (95% CI 0.185 to 0.243) and 0.172 (95% CI 0.154 to 0.190) in the European samples (CREAM-EUR and 23andMe), while it was only 0.053 (95% CI -0.025 to 0.131) in the Asian sample (CREAM-EAS). Next, we estimated the genetic correlation between Europeans and Asians by comparing variant effect size for common variants using the novel statistical program Popcorn[48]. Popcorn takes summary GWAS statistics from two populations and LD information from ancestry-matched reference panels, and computes genetic correlations by implementing a weighted likelihood function that accounts for the inflation of Z scores due to LD (Online Methods). Two genetic correlation metrics were calculated (Table 2); first, a genetic effect correlation (ρge) that quantifies the

correlation in SNP effect sizes between Europeans and Asians without taking into account ancestry-related differences in allele frequency; and second, a genetic impact correlation (ρgi) that estimates the correlation in variance-normalized SNP effect sizes between the two ancestry groups. Estimates of the genetic effect correlation ρge were high between Europeans and Asians, but significantly different from 1 (0.79 and 0.80 respectively at $P < 1.9 \times 10^{-6}$; Table 2), indicating a clear genetic overlap but a difference in per allele effect size. Estimates of the genetic impact correlation ρgi were similarly high (> 0.8), but not significantly different from 1 for the correlation between CREAM-EUR and CREAM-ASN ($P = 0.065$), indicating that the genetic impact of these alleles may still be similar.

In silico pathway analysis

We used an array of bioinformatics tools to investigate potential functions and pathways of the associated genes. We first employed DEPICT[49] to perform a gene set enrichment analysis, a tissue type enrichment, and a gene prioritization analysis, on all variants with P value < 1.00×10^{-5} from Stage 3. The gene set enrichment analysis resulted in 66 reconstituted gene sets, of which 55 (83%) were eye-related. To reduce redundancies between pathways, we clustered the significant pathways into 13 meta gene sets (false discovery rate (FDR) < 5% and a P value < 0.05) (Supplementary Methods 1, Figure 4, Supplementary Excel File 4). The most significant gene set was the 'abnormal photoreceptor inner segment morphology' (MP:0003730; P value = 1.79×10^{-7}). The eye-related meta gene sets consisted of the 'thin retinal outer nuclear layer' (MP:0008515; 27 (55%) gene sets), 'detection of light stimulus' (GO:0009583; 13 (24%) gene sets), 'nonmotile primary cilium' (GO:0031513; 4 (6%) gene sets), and 'abnormal anterior eye segment morphology' (MP:0005193; 4 (6%) gene sets). The first three meta gene sets had a Pearson's correlation > 0.6. Interestingly, *RGR*, *RP1L1*, *RORB* and *GNB3* were present in all of these meta gene sets. Retina was the most significant tissue of expression according to the tissue enrichment analysis (P value = 1.11×10^{-4}, FDR <0.01). From the gene prioritization according to DEPICT, 7 genes were

highlighted as the most likely causal genes at *P* value < 7.62 x 10-6 and FDR <0.05: *ANO2, RP1L1, GNB3, EDN2, RORB* and *CABP4*.

Next, we performed a canonical pathway analysis on all genes annotated to the variants of Stage 3 using Ingenuity Pathway Analysis (IPA; http://www.ingenuity.com/index.html). All genes were run against the IPA database incorporating functional biological evidence on genomic and proteomic expression based on regulation or binding studies. IPA identified "Glutamate Receptor Signaling" with central player *Nf-kB* gene as the most significant pathway after correction for multiple testing (ratio of the number of molecules 8.8% and Fisher's Exact test *P* value = 1.56×10^{-4}; Figure 5, Supplementary Figure 10).

From disease associated loci to biological mechanisms

We adapted the scoring scheme designed by Fritsche et al.[50] to highlight genes for which there is biological plausibility for a role in eye growth. We used 10 equally rated categories (maximum score 10; genes with score ≥ 5 Table 3; all genes Supplementary Excel File 5; Online Methods, Supplementary Methods 1): internal replication of index genetic variants in the individual cohort GWAS (CREAM-ASN, CREAM-EUR and 23andMe), evidence for an eQTL effect in at least four tissue or cell types, annotation to altered genomic function, ocular phenotype in humans and in mice, expression in human adult and fetal ocular tissue, the presence of genes in the gene set enrichment, the presence of genes in the prioritization analysis of DEPICT, and the presence of genes in the top 5 canonical pathway analysis of IPA. Sixty-five index variants replicated in two or more individual cohorts; we found evidence for seven genetic variants with eQTL effects in multiple tissue types; nine exonic variants, of which seven predicted protein-alterations (Supplementary Table 4); 27 RNA genes, six located in the 3' or 5'UTR (Supplementary Table 7, Supplementary Figure 11), 84 genes resulting in an ocular phenotype in humans (Supplementary Excel File 6) and 28 in mice (Supplementary Excel File 7); 169/212 (79%) genes expressed in human ocular tissue (Supplementary Methods 1, Supplementary Excel File 8); 42 genes identified by DEPICT at *P*

value < 5.4 x 10^{-4} and FDR < 0.05 and 45 genes contributed to the most significant canonical pathways of IPA. Notably, 48 of the associated genes encode known drug targets (Supplementary Excel File 9).

The gene with the highest biological plausibility score (score = 8) was *GNB3*, a highly conserved gene encoding a guanine nucleotide-binding protein expressed in rod and cone photoreceptors and ON-bipolar cells[51]. *GNB3* participates in signal transduction through G-protein coupled receptors and enhances the temporal accuracy of phototransduction and ON-center signaling in the retina[51]. As described above, the index SNP harbors a missense variant associated with refractive errors. Non-synonymous mutations within *GNB3* are known to cause syndromic congenital stationary night blindness[52] in humans, progressive retinopathy and globe enlargement in chickens[51], and abnormal development of the photoreceptor-bipolar synapse in knock-out mice[53,54].

Other genes highly ranked (score = 7) include *CYP26A1*, *GRIA4*, *RDH5*, *RORB* and *RGR*, all previously associated with refractive error, and one newly identified gene: *EFEMP1*. *EFEMP1* encodes a member of the fibulin family of extracellular matrix glycoproteins, and is found pan-ocularly including in the inner nuclear layer and Bruch's membrane. Mutations in this gene lead to specific macular dystrophies[55], while variants have also been shown to co-segregate with primary open-angle glaucoma[56] and associate with optic disc cup area[57].

Several other genes from our analysis are noteworthy for their function. *CABP4*, a calcium binding protein expressed in cone and rod photoreceptor cells, mediates Ca^{2+} influx and glutamate release in the photoreceptor-bipolar synapse[58]. Mutations in this gene have been described in congenital cone-rod synaptic disorder[59], a retinal dystrophy associated with nystagmus, photophobia, and, remarkably, high hyperopia. *KCNMA1* encodes pore forming alpha subunits of Ca^{2+}-activated K^+ (BK) channels. These channels regulate synaptic transmission exclusively in the rod pathway[60]. A striking function of the other previously identified genes is retinoic acid signaling and metabolism[61-63]. *ANO2* is a Ca^{2+}-activated Cl^- channel recently reported to regulate retinal pigment epithelial (RPE) cell volume in a light-dependent manner[64]. *EDN2* is a potent vasoconstrictor that binds to two G-protein-coupled receptors, *EDNRA*, which resides on bipolar dendrites, and *EDNRB*, which is present on Mueller and horizontal cells. Both receptors

are also present on choroidal vessels[65], implying that the choroid as well as retinal cells are target sites for this gene. *RP1L1* is expressed in cone and rod photoreceptors where it is involved in the maintenance of microtubules in the connecting cilium[66]. Mutations in this gene cause dominant macular dystrophy and retinitis pigmentosa[67]. We replicated two genes known to cause myopia in family studies. *FBN1* harbors mutations causing with Marfan (OMIM #154700) and Weil Marchesani (OMIM #608328) syndrome; *PTPRR* was one of the candidates in the MYP3 locus, which was found by linkage in families with high myopia[68].

The location of rs7449443 (*P* value 3.58 x 10^{-8}) is notable as it resides in between *DRD1* and *FLJ16171*. *DRD1* encodes dopamine receptor 1 and is known to modulate dopamine receptor 2-mediated events[69,70]. The dopamine pathway has been implicated in myopia pathogenesis in many studies[69,71]. SNPs in and near other genes involved in the dopamine pathway (dopamine receptors, synthesis, degradation, and transporters)[72-74] did not reveal genome-wide significant associations (Supplementary Methods 2, Supplementary Table 8; Supplementary Figure 12).

There were twenty-eight genetic variants in or near DNA structures transcribing RNA genes (non coding RNA, linc RNAs, tRNAs, snoRNas, rRNAs). Notably, five were in the transcription region and thirteen were in the vicinity (>0 kb and ≤ 50 kb) of start or end of the RNA gene transcription region. They received low scores, since many have no reported function or disease association to date (Table 3, Supplementary Excel File 10, Supplementary Figure 11, Supplementary Table 7). Our ranking of genes based on functional information existing in the public domain does not necessarily represent the true order of importance for refractive error pathogenesis. The observation that genes with strong statistical association were distributed over all scores supports this concept. Nevertheless, this list may help to select genes for subsequent functional studies.

Finally, integration of all aforementioned data with findings from literature allowed us to annotate a large number of genes to ocular cell types (Figure 6). Remarkably, all cell types of the retina harbored refractive error genes, as well as the RPE, vascular endothelium, and extracellular matrix.

Genetic pleiotropy

We performed a GWAS catalogue look up using FUMA to investigate overlap of genes with other common traits (Supplementary Figure 13)[75]. Refractive error and hyperopia were replicated significantly after correcting for multiple testing (adjusted *P* value 1.44×10^{-52} and 9.34×10^{-9}, respectively). We found significant overlap with 74 other traits, of which height (adjusted *P* value 1.11×10^{-10}), obesity (adjusted *P* value 1.38×10^{-10}), and BMI (adjusted *P* value 4.05×10^{-7}) were most important. Ocular traits significantly associated were glaucoma (optic cup area, intraocular pressure; adjusted *P* values 2.69×10^{-5} and 3.01×10^{-5}, respectively) and age-related macular degeneration (adjusted *P* value 1.27×10^{-3}).

DISCUSSION

Myopia may become the leading cause of world blindness in the near future, a grim outlook for which current counteractions are still insufficient[11,76]. To improve understanding of the genetic landscape and biology of the refractive error trait, we conducted a large GWAS meta-analysis in 160,420 participants of mixed ancestry and replicated in 95,505 participants. This led to the identification of 139 independent susceptibility loci by single variant analysis and 22 additional loci through post-GWAS methods, a four-fold increase in refractive error genes. The majority of annotated genes were found to be expressed in the human posterior segment of the eye. Using in silico analysis, we identified significant biological pathways, of which retinal cell physiology, light processing, and specifically glutamate receptor signaling were the most prominent mechanisms. Our integrated bio-informatic approach highlighted known ocular functionality for many genes.

To ensure robustness of our genetic associations, we included studies of various designs and populations, sought replication in an independent cohort of significant sample size, and stringently accounted for population stratification by performing genomic control at all stages of the meta-analysis[77].

With this approach, we internally replicated all loci from CREAM in 23andMe, and replicated a considerable proportion of the 23andMe loci in CREAM. We combined studies with outcomes based on actual refractive error measurements as well as on self-reported age-of-myopia-onset, and found the direction-of-effect of the associated variants, as well as their effect size, to be remarkably consistent. Combining two different outcome measures may appear unconventional, but age of onset and refractive error have been shown to be very tightly correlated[11,28]. Each year of earlier onset leads to a higher degree of myopia[78,79]. Moreover, the high genetic correlation of common SNPs between the two phenotypes underscores their similarity. Most compelling evidence was provided by replication of 86% of the discovered variants in the independent UKEV cohort which also used conventional refractive error measurements. This robustness indicates that both phenotypic outcomes (SphE and AODM) can be used to capture a shared source of genetic variation. In addition, we found trans-ethnic replication of significant loci, and a high per-allele correlation of genetic effects of common variants in the Europeans and Asians. Our findings support a largely shared genetic predisposition to refractive error and myopia in the two ethnicities, although ancestry-specific allelic effects may exist. The low heritability estimate in Asians may, in part, be explained by the low representation of this ethnicity in our study sample. Alternatively, it may imply that environmental factors explain a greater proportion of the phenotypic risk and recent rise in myopia prevalence in this ancestry group[80].

Limitations of our study were the possibility of false negative findings due to genomic control, and underrepresentation of studies with Asian ancestry. Heterogeneity of observed effect estimates was large for several associated variants, but not unexpected given the large number of collaborating studies with varying methodology.

Although neurotransmission was already a suggested pathway in our previous studies[26,27], our current pathway analyses provide more in depth insights into the retinal circuitry driving refractive error. DEPICT identified ‘thin retinal outer nuclear layer’, ‘detection of light stimulus’, and ‘nonmotile primary cilium’ as the most important meta-gene sets. These are the main characteristics of photoreceptors, which are located in the outer retina and contain cilia. These photosensitive cells drive the phototransduction

cascade in response to light, which in turn induces visual information processing. IPA pointed towards glutamate receptor signaling as the most significant pathway. Glutamate is released by photoreceptors and determines conductance of retinal signaling to the ON and OFF bipolar cells[81]. Our functional gene look ups provide evidence that rod as well as cone bipolar cells play a role (rod: *CLU*; cone: *GNB3*). Taken together, these findings strongly suggest that light response and light processing in the retina are initiating factors leading to refractive error.

The genetic association with light dependent pathways may also link to the well-established protective effect of outdoor exposure on myopia. We found suggestive evidence for a genetic association with *DRD1*, the dopamine receptor D1 gene. The dopaminergic pathway has been studied extensively in animal models for its role in controlling eye growth in response to light[69,71,82-91]. *DRD1* was found to be a mediator in this process, as bright light increased DRD1 activity in the bipolar ON-pathway, and diminished form deprivation myopia in mice. Blockage of DRD1 reversed this inhibitory effect[92]. We did not find evidence for direct involvement of other genes in the dopamine pathway, but *GNB3* may be an indirect modifier as it is a downstream signaling molecule of dopamine and has been shown to influence availability of the dopamine transporter DAT[93]. Although a promising target for therapy, further evidence of *DRD1* in human myopiagenesis is warranted.

Novel pathways elicited by the newly identified genes are anterior segment morphology *(TCF7L2, VIPR2, MAF*) and angiogenesis (*FLT1*). In addition, the high number of variants residing near small RNA genes suggests that post-transcriptional regulation is an important mechanism, as these RNAs are known to play a distinct and central regulatory role in cells[94]. These findings will serve as leads for future studies performing detailed mapping of cellular networks, and functional studies into genes implicated in ocular phenotypes, harboring protein-altering variants, and proven drug targets.

Our evaluation of shared genetics between refractive error and other disease-relevant phenotypes highlighted overlap with anthropometric traits such as height, obesity, and BMI. This could give valuable additional clues as to the phenotypic outcomes of perturbations of some of the networks identified.

Our genetic observations add credence to the current notion that refractive errors are caused by a retina-to-sclera signaling cascade that induces scleral remodeling in response to light stimuli. The concept of this cascade originates from various animal models showing that form deprivation, retinal defocus and contrast, ambient light, and wavelength can influence eye growth in young animals[95-97]. Cell-specific moieties in this putative signaling cascade in humans were largely unknown, although animal models implicated GABA, dopamine, all-trans-retinoic acid and TGF-β[69,91,98,99]. Our study provides a large number of new molecular candidates for this cascade, and clearly shows that a wide range of neuronal cell types in the retina, the RPE, the vascular endothelium, as well as components of the extracellular matrix are implicated (Figure 6). The many interprotein relationships (Figure 4) exemplify the complexity of eye growth, and provide a challenge to develop strategies to prevent pathological eye elongation.

In conclusion, by using a cross-ancestry design in the largest study population on common refractive errors to date, we uncovered numerous novel loci and pathways involved in eye growth. Our multi-disciplinary approach incorporating GWAS data with *in silico* analyses and expression experiments provides an example for the design of future genetic studies for complex traits. Additional genetic insights into refractive errors will be gained by increasing sample size, greater genotyping depth, family studies for identifying rare alleles of large effect, and by evaluating population extremes. Our list of plausible genes and pathways provide a plethora of data for future studies focusing on gene-environment interaction, and on translation of GWAS findings into starting points for therapy.

ONLINE METHODS

Ethics Statement

All human research was approved by the relevant institutional review boards and conducted according to the Declaration of Helsinki. All CREAM participants provided written informed consent; all 23andMe applicants provided informed consent online, and answered surveys according to 23andMe's human subjects protocol, which was reviewed and approved by Ethical & Independent Review Services, an AAHRPP-accredited institutional review board.

Study data

The study populations were participants of the Consortium for Refractive Error and Myopia (CREAM) comprising of 41,793 individuals with European ancestry from 26 cohorts (CREAM-EUR) and 11,935 individuals with Asian ancestry from 8 studies (CREAM-ASN); and customers of the 23andMe genetic testing company who gave informed consent for inclusion in research studies consisting of 104,293 individuals (2 cohorts of individuals with European ancestry, N = 12,128 and N= 92,165, respectively). All participants included in this analysis from CREAM and 23andMe were aged 25 years or older. Participants with conditions that could alter refraction, such as cataract surgery, laser refractive procedures, retinal detachment surgery, keratoconus as well as ocular or systemic syndromes were excluded from the analyses. Recruitment and ascertainment strategies varied per study (Supplementary Table 1a,b, and Supplementary Methods 3). Refractive error represented by measurements of refraction and analyzed as spherical equivalent (SphE =spherical refractive error + 1/2 cylinder refractive error) was the outcome variable for CREAM; myopic refractive error represented by self-reported age of diagnosis of myopia (AODM) for 23andMe[27].

Genotype calling and imputation

Samples were genotyped on different platforms and study specific quality control measures of the genotyped variants were implemented before association analysis (Supplementary Table 1a). Genotypes were imputed using the appropriate ancestry-matched reference panel for all cohorts from the 1000 Genomes Project (Phase I version 3, March 2012 release) with either minimac[100] or IMPUTE[101,102]. The metrics for pre-imputation quality control varied amongst studies, but genotype call rate thresholds were set at high level (≥0.95 for both CREAM and 23andMe). These metrics were similar to our previous GWAS analyses[26,27]; details per cohort can be found in Supplementary Table 1a.

GWAS per study

For each CREAM cohort, a single marker analysis for the SphE (in diopters) phenotype was carried out using linear regression adjusting for age, sex and up to the first five principal components. All non-family-based cohorts removed one of each pair of relatives (after detection using either GCTA or IBS/IBD analysis). In family-based cohorts, a score test-based association was used to adjust for within-family relatedness[103,104]. For the 23andMe participants, Cox proportional hazards analysis testing AODM as the dependent variable were performed as previously described[27], with *P* values calculated using a likelihood ratio test for the single marker genotype term. We used an additive SNP allelic effect model for all analyses.

Centralized quality control per study

After individual GWAS, all studies underwent a second round of quality control (QC). Quantile-quantile, effect allele frequency, *P* – *Z* test, standard error – sample size, and genomic control inflation factor plots were generated for each individual cohort using EasyQC[105] (Supplementary Figure 2.1, 2.2, 2.3) . All analytical issues discovered during this QC step were resolved per individual cohort.

GWAS meta-analyses

The GWAS meta-analyses were performed in three stages (Supplementary Figure 1). In Stage 1, European (CREAM-EUR) and Asian (CREAM-ASN) participants from the CREAM cohort were meta-analysed separately. Subsequently, all CREAM cohorts (CREAM-ALL) were meta-analysed. Variants with MAF < 1% or imputation quality score < 0.3 (info metric of IMPUTE) or Rsq < 0.3 (minimac) were excluded. A fixed effects inverse variance-weighted meta-analysis was performed using METAL[106]. In all stages, each genetic variant had to be represented by at least half of the entire study population and at least represented by 13 cohorts in CREAM and one cohort in 23andMe. For SNPs with high heterogeneity (at $P < 0.05$), we also performed a random effects meta-analysis using METASOFT[50]. In Stage 2, a meta-analysis of the two 23andMe cohorts was performed, using similar filtering but a lower MAF threshold (< 0.5%). In Stage 3, CREAM-ALL and 23andMe samples were combined using a fixed effects meta-analysis based on *P* values and direction of effect.

In Stage 3, we chose a different weighting scheme due to the differences in effect size scaling; 23andMe used a less accurate phenotype variable (AODM); i.e. the *effective* sample size of the 23andMe was approximately equivalent to the *effective* sample size of CREAM-ALL (Figure 2b), thus weighting by $(1/\sqrt{n_{effective}})$ yielded a final weighting ratio of 1:1[107,108]. Genome-wide statistical significance was defined at $P < 5.0 \times 10^{-8}$ [109]. All three meta-analysis stages were performed under genomic control. Study specific and meta-analysis lambda (λ) estimates are shown in Supplementary Figure 7; to check for confounding biases (e.g. cryptic relatedness and population stratification), LD score intercepts from LD score regressions per ancestry were constructed (Supplementary Figure 8)[30]. To check the robustness of signals, we performed a conventional random effects models using METASOFT, fixed effects models weighted on sample size and on weights estimated from standard error per allele tested using METAL (Supplementary Excel Files 1 and Supplementary Excel Files 2).

Manhattan (modified version of package 'qqman'), regional, box, and forest plots were made using R version 3.2.3 and LocusZoom[110]. An overview of the Hardy Weinberg *P* values of all index variants per

cohort can be found in Supplementary Excel File 3. The comparison between refractive error and age-of-onset was performed using the LDSC program[30].

Population stratification and heritability calculations

Each study assessed the degree of genetic admixture and stratification in their study participants through the use of principal components. Homogeneity of participants was assured by removal of all individuals whose ancestry did not match the prevailing ancestral group. We used genomic inflation factors to control for admixture and stratification, and performed genomic-controlled meta-analysis to account for the effects of any residual heterogeneity. To further distinguish between inflation from a true polygenic signal and population stratification, we examined the relationship between test statistics and linkage disequilibrium (LD) with LDSC. CREAM-EUR, CREAM-ASN and 23andMe were evaluated separately; variants not present in HapMap3 and MAF < 1% were excluded. SNP heritability estimates were calculated using LDSC for the same set of genetic variants.

Locus definition and annotation

All study effect size estimates were oriented to the positive strand of the NCBI Build 37 reference sequence of the human genome. The index variant of a locus was defined as the variant with the lowest *P* value in a region spanning a 100 kb window of the most outer genome wide significant variant of that same region. We annotated all index variants using the web-based version of ANNOVAR[111]based on UCSC Known Gene Database[35]. For variants within the coding sequence or 5' or 3' untranslated regions of a gene, that gene was assigned to the index variant (note that this led to more than 1 gene being assigned to variants located within the transcription units of multiple, overlapping genes). For variants in intergenic regions, the nearest 5' gene and the nearest 3' gene were assigned to the variant. Index variants were annotated to functional RNA elements when described as such in the UCSC Known Gene Database.

We used conservation (PhyloP[112]) and prediction tools (SIFT[39], Mutation Taster[113], align GVGD[40,41], PolyPhen-2[36]) to predict the pathogenicity of protein-altering exonic variants.

Conditional signal analysis

We performed conditional analysis to identify additional independent signals nearby the index variant at each locus, using GCTA-COJO[32]. We transformed the Z-scores of the summary statistics to beta's using the following formula: Standard Error = $\sqrt{1/2 * N * MAF(1 - MAF)}$. We performed the GCTA-COJO analysis[32], utilizing summary-level statistics from the meta-analysis on all cohorts. Linkage disequilibrium (LD) between variants was estimated from the Rotterdam Study I-III.

Replication in UK Biobank

The UK Biobank Eye & Vision (UKEV) Consortium performed a GWAS of refractive error in 95,505 participants of European ancestry aged 37-73 year with no history of eye disorders[33]. Refractive error was measured using an autorefractor; SphE was calculated per eye and averaged between the two eyes. To account for relatedness a mixed model analysis with BOLT-LMM was used[114], including age, gender, genotyping array, and the first 10 principal components as covariates. Analysis was restricted to markers present on the HRC reference panel[115]. We performed lookups for all independent genetic variants identified in our Stage 3 meta-analysis and conditional analysis. For variants not present in UKEV, we performed lookups for a surrogate variant in high LD (r^2 >0.8). When more than one potential surrogate variant was available, the variant in strongest LD with the index variant was selected.

Post-GWAS analyses

We performed two gene-based tests to identify additional significant genes not found in the single variant analysis. First, we applied the gene-based test implemented in fastBAT[42] to the per-variant summary statistics of the meta-analysis of all European cohorts (23andMe and CREAM-EUR). We used the default

parameters (all variants in or within 50kb of a gene) and focused on variants with a gene-based *P* value $<2 \times 10^{-6}$ (Bonferroni correction based on 25,000 genes) and the per-variant *P* value $>5 \times 10^{-8}$. Secondly, we applied another gene-based test in EUGENE[43] which only includes variants which are eQTLs (GTex, blood[116]). EUGENE tests an hypothesis predicated on eQTLs as key drivers of the association signal. eQTLs within 50kb of a gene were included in the test. Genes with EUGENE *P* value $<2 \times 10^{-6}$ (and not found in the single variant analysis) were considered to be significant. Finally, we used functional annotation information from genome-wide significant loci to reweigh results using fgwas (version 0.3.64[44]). This approach is able to identify risk loci that otherwise might not reach the genome-wide significance threshold in standard GWAS. Details about this approach can be found in Supplementary Methods 4.

Refractive errors and myopia risk prediction

To assess the risk of the entire range of refractive errors, we computed polygenic risk scores (PGRS) for the population-based Rotterdam Studies (RS) I, RS-II and RS-III using the *P* values and *Z* scores from a meta-analysis on CREAM-ALL and 23andMe, excluding the RS I-III cohorts. Only variants with high imputation quality (IMPUTE info score > 0.5 or minimac Rsq > 0.8) and MAF > 1% were considered. *P* value-based clumping was performed with PLINK[117], using an r^2 threshold of 0.2 and a physical distance threshold of 500 kb, excluding the MHC region. This resulted in a total of 243,938 variants. For each individual in RS-I, RS-II and RS-III (*N* = 10,792), PGRS were calculated using the --score command in PLINK across strata of *P* value thresholds: 5.0×10^{-8}, 5.0×10^{-7}, 5.0×10^{-6}, 5.0×10^{-5}, 5.0×10^{-4}, 0.005, 0.01, 0.05, 0.1, 0.5, 0.8 and 1.0. The proportion of variance explained by each PGRS model was calculated as the difference in the R^2 between two regression models; one where SphE was regressed on age, sex, the first five principal components, and the other also including the PGRS as an additional

672 covariate. Subsequently, AUCs were calculated for myopia (SphE ≤ -3 SD) versus hyperopia (SphE ≥ +3
673 SD).
674
675 ## Genetic correlation between ancestries
676 We used Popcorn[48] to investigate ancestry-related differences in the genetic architecture of refractive
677 error and myopia. Pairwise analyses were carried out using the GWAS summary statistics from 23andMe
678 (*N* = 104,292), CREAM-EUR (*N* = 44,192) and CREAM-EAS (*N* = 9,826) meta-analyses. Only SNPs
679 with MAF ≥ 5% were included, resulting in a final set of 3,625,602 SNPs for analyses involving
680 23andMe and 3,642,928 SNPs for the CREAM-EUR versus CREAM-EAS analysis. Reference panels
681 were constructed using genotype data from 503 European and 504 East Asian individuals sequenced as
682 part of the 1000 Genomes Project (release 2013-05-02 downloaded from: ftp.1000genomes.ebi.ac.uk).
683 The reference panel VCF files were filtered using PLINK[117] to remove indels, strand-ambiguous variants,
684 variants without an "rs" id prefix, and variants located in the MHC region on chromosome 6
685 (chr6:25,000,000-33,500,000; Build 37).
686
687 ## Analysis between phenotypes
688 To evaluate consistency of genotypic effects across studies that employed different phenotype definitions,
689 we compared effect sizes from GWAS studies of either SphE or AODM in Europeans, i.e. CREAM-EUR
690 (*N* = 44,192) or 23andMe (*N* = 104,293) respectively. Marker-wise additive genetic effect sizes (in units
691 diopters per copy of the risk allele) for SphE were compared against those (in units log(HR) per copy of
692 the risk allele) for AODM. Data was visualised using R. Genetic correlation between the two phenotypes
693 SphE and AODM was calculated using LD score regression. This analysis included all common SNPs
694 (MAF > 0.01) present in HapMap3.
695
696 ## Evidence for functional involvement

In order to rank genes according to biological plausibility, we scored annotated genes based on our own findings and published reports for a potential functional role in refractive error. Points were assigned for each gene on the basis of 10 categories (details on the methodology per category are provided in Supplementary Methods 3): internal replication of index genetic variants in the individual cohort GWAS analyses through Bonferroni corrections (CREAM-ASN, CREAM-EUR and 23andMe; *pBonferroni* 1.10 x 10^{-4}), evidence for eQTL using the FUMA[32] and extensive look-ups in GtEx, evidence of expression in the eye in developmental and adult ocular tissues, presence of an eye phenotype in knock-out mice (MGI and IMPC database), presence of an eye phenotype in humans (OMIM[118] (http://omim.org), DisGeNET[119]), location in a functional region of a gene (wANNOVAR), presence of the gene in a significant enriched functional pathway with false discovery rate < 0.05 (DEPICT[49]), presence of the gene in the gene priority analysis of DEPICT with false discovery rate < 0.05 and the presence of the gene in the canonical pathway analysis of Ingenuity Pathway Analysis (IPA; http://www.ingenuity.com/index.html). Furthermore, we performed a systematic search for each gene to assess its potential as a drug target (SuperTarget[120], STITCH[121], DrugBank[122], PharmaGkb[123]). All information derived from this study and literature were used to annotate genes to retinal cell types.

Genetic pleiotropy

To investigate overlap of genes with other common traits, we performed a look-up in the GWAS catalog using FUMA. Multiple testing correction (i.e. Benjamini-Hochberg) was performed. Traits were significantly associated when adjusted *P* value ≤ 0.05 and the number of genes that overlap with the GWAS catalog gene sets was ≥ 2.

Data availability statement

The summary statistics of the Stage 3 meta-analysis are included in supplementary information files of this published article. In order to protect the privacy of the participants in our cohorts, further summary statistics of Stage 1 (CREAM) and Stage 2 (23andMe) will be available upon request. Please contact

c.c.w.klaver@erasmusmc.nl (CREAM) and/or apply.research@23andMe.com (23andMe) for more information and to access the data.

Acknowledgments

We gratefully thank the invaluable contributions of all study participants, their relatives and staff at the recruitment centers. Complete funding information and acknowledgments by study can be found in the **Supplementary Note**.

Author contributions

M.S.T., V.J.M.V., S.M., J.A.G., A.I.I.G., R.W., P.G.H., A.I.I.G., and E.M.v.L. performed the analyses. C.C.W.K., V.J.M.V., M.S.T., R.W., J.A.G., and S.M. drafted the manuscript, and C.J.H., P.G.H., A.P.K., C.M.v.D., D.S, E.M.v.L., J.E.B.W., J.T., N.A.F., Q.F., S.M.S., and V.V. critically reviewed the manuscript. A.N., A.P.K., A.T., C.B., C.Gi., C.L.S., C.Y.C., G.Bi., G.C., I.R., J.E.B.W., J.E.H., J.S.Ri., J.W., J.X., K.M.W., K.Y., M.P.C., M.S.H., M.S.T., N.A.F., N.E., P.C., P.Gh., P.K.J., Q.F., R.Ho., R.L.S., R.P.I., R.W., T.H., T.H.S.A., T.Z., V.V., W.Y.S., W.Z., X.L.S., Y.C.H., Y.S., and Y.Y.T. performed data analysis for the individual studies; and A.D.P., A.G.U., A.T., A.W.H., B.E.K.K., C.C.W.K., C.D., C.H., C.J.H., C.W., C.Y.C., D.A.M., F.R., G.Be., H.M.H., J.A.G., J.B.J., J.E.B.W., J.E.C., J.F.W., J.H.L., J.R.V., J.S.Ra., J.S.Ri., J.T., K.Y., M.A.M.S., N.G.M., N.P., O.Po., O.Pa., O.T.R., P.Gu., P.J.F., P.M., P.N.B., R.K., S.K.I., S.M.S., T.L., T.M., W.Z., Y.C.H., and Y.X.W. contributed to data assembly. A.A.B.B., A.W., C.Gr., D.S., K.N.W., S.W.J.T., and T.Y. performed expression experiments, and M.S.T., A.A.B.B., P.J.v.d.S., and R.Ha. performed in silico pathway analyses. C.C.W.K. and C.J.H. conceived and designed the outline of the current report, and jointly with A.M., A.H., A.W.H., C.D., C.H., C.J.H., C.M.v.D., C.W., C.Y.C., D.A.M., D.S., E.S.T., F.M., G.Bi., I.R., J.A.G., J.B.J., J.E.B.W., J.E.C., J.F.W., J.H.L., J.R.V., J.T., N.A., N.A.F., N.P., O.Pa., O.T.R., P.J.F., P.N.B., S.K.I., S.M.S., T.L., T.Y.W., T.Y., V.V., Y.X.W., and Y.Y.T. supervised conduction of experiments and analyses.

References

1. Pan, C.W., Ramamurthy, D. & Saw, S.M. Worldwide prevalence and risk factors for myopia. *Ophthalmic Physiol Opt* **32**, 3-16 (2012).
2. Morgan, I.G. What Public Policies Should Be Developed to Deal with the Epidemic of Myopia? *Optom Vis Sci* **93**, 1058-60 (2016).
3. Morgan, I. & Rose, K. How genetic is school myopia? *Prog Retin Eye Res* **24**, 1-38 (2005).
4. Morgan, I.G., Ohno-Matsui, K. & Saw, S.M. Myopia. *Lancet* **379**, 1739-48 (2012).
5. Williams, K.M. *et al.* Increasing Prevalence of Myopia in Europe and the Impact of Education. *Ophthalmology* **122**, 1489-97 (2015).
6. Williams, K.M. *et al.* Prevalence of refractive error in Europe: the European Eye Epidemiology (E(3)) Consortium. *Eur J Epidemiol* **30**, 305-15 (2015).
7. Vongphanit, J., Mitchell, P. & Wang, J.J. Prevalence and progression of myopic retinopathy in an older population. *Ophthalmology* **109**, 704-11 (2002).
8. Seet, B. *et al.* Myopia in Singapore: taking a public health approach. *Br J Ophthalmol* **85**, 521-6 (2001).
9. Smith, T.S., Frick, K.D., Holden, B.A., Fricke, T.R. & Naidoo, K.S. Potential lost productivity resulting from the global burden of uncorrected refractive error. *Bull World Health Organ* **87**, 431-7 (2009).
10. Verhoeven, V.J. *et al.* Visual consequences of refractive errors in the general population. *Ophthalmology* **122**, 101-9 (2015).
11. Tideman, J.W. *et al.* Association of Axial Length With Risk of Uncorrectable Visual Impairment for Europeans With Myopia. *JAMA Ophthalmol* **134**, 1355-1363 (2016).
12. Flitcroft, D.I. The complex interactions of retinal, optical and environmental factors in myopia aetiology. *Prog Retin Eye Res* **31**, 622-60 (2012).
13. Nakanishi, H. *et al.* A genome-wide association analysis identified a novel susceptible locus for pathological myopia at 11q24.1. *PLoS Genet* **5**, e1000660 (2009).
14. Lam, C.Y. *et al.* A genome-wide scan maps a novel high myopia locus to 5p15. *Invest Ophthalmol Vis Sci* **49**, 3768-78 (2008).
15. Stambolian, D. *et al.* Meta-analysis of genome-wide association studies in five cohorts reveals common variants in RBFOX1, a regulator of tissue-specific splicing, associated with refractive error. *Hum Mol Genet* **22**, 2754-64 (2013).
16. Fan, Q. *et al.* Genetic variants on chromosome 1q41 influence ocular axial length and high myopia. *PLoS Genet* **8**, e1002753 (2012).
17. Fan, Q. *et al.* Meta-analysis of gene-environment-wide association scans accounting for education level identifies additional loci for refractive error. *Nat Commun* **7**, 11008 (2016).
18. Cheng, C.Y. *et al.* Nine Loci for Ocular Axial Length Identified through Genome-wide Association Studies, Including Shared Loci with Refractive Error. *Am J Hum Genet* **93**, 264-77 (2013).
19. Shi, Y. *et al.* Exome sequencing identifies ZNF644 mutations in high myopia. *PLoS Genet* **7**, e1002084 (2011).
20. Shi, Y. *et al.* Genetic variants at 13q12.12 are associated with high myopia in the Han Chinese population. *Am J Hum Genet* **88**, 805-13 (2011).
21. Li, Y.J. *et al.* Genome-wide association studies reveal genetic variants in CTNND2 for high myopia in Singapore Chinese. *Ophthalmology* **118**, 368-75 (2011).
22. Li, Z. *et al.* A genome-wide association study reveals association between common variants in an intergenic region of 4q25 and high-grade myopia in the Chinese Han population. *Hum Mol Genet* **20**, 2861-8 (2011).
23. Liu, J. & Zhang, H.X. Polymorphism in the 11q24.1 genomic region is associated with myopia: a comprehensive genetic study in Chinese and Japanese populations. *Mol Vis* **20**, 352-8 (2014).

24. Tran-Viet, K.N. *et al.* Mutations in SCO2 are associated with autosomal-dominant high-grade myopia. *Am J Hum Genet* **92**, 820-6 (2013).
25. Aldahmesh, M.A. *et al.* Mutations in LRPAP1 are associated with severe myopia in humans. *Am J Hum Genet* **93**, 313-20 (2013).
26. Verhoeven, V.J. *et al.* Genome-wide meta-analyses of multiancestry cohorts identify multiple new susceptibility loci for refractive error and myopia. *Nat Genet* (2013).
27. Kiefer, A.K. *et al.* Genome-wide analysis points to roles for extracellular matrix remodeling, the visual cycle, and neuronal development in myopia. *PLoS Genet* **9**, e1003299 (2013).
28. Wojciechowski, R. & Hysi, P.G. Focusing in on the complex genetics of myopia. *PLoS Genet* **9**, e1003442 (2013).
29. Genomes Project, C. *et al.* A global reference for human genetic variation. *Nature* **526**, 68-74 (2015).
30. Bulik-Sullivan, B.K. *et al.* LD Score regression distinguishes confounding from polygenicity in genome-wide association studies. *Nat Genet* **47**, 291-5 (2015).
31. Yang, J. *et al.* Genomic inflation factors under polygenic inheritance. *Eur J Hum Genet* **19**, 807-12 (2011).
32. Watanabe, K., Taskesen, E., van Bochoven, A. & Posthuma, D. FUMA: Functional mapping and annotation of genetic associations. *bioRxiv* (2017).
33. Plotnikov, D., Guggenheim, J. & Is a large eye size a risk factor for myopia? A Mendelian randomization study. *bioRxiv* (2017).
34. UCSC Genome Browser.
35. Hsu, F. *et al.* The UCSC Known Genes. *Bioinformatics* **22**, 1036-46 (2006).
36. Adzhubei, I.A. *et al.* A method and server for predicting damaging missense mutations. *Nat Methods* **7**, 248-9 (2010).
37. Ng, P.C. & Henikoff, S. SIFT: Predicting amino acid changes that affect protein function. *Nucleic Acids Res* **31**, 3812-4 (2003).
38. Kelly, M.P. Does phosphodiesterase 11A (PDE11A) hold promise as a future therapeutic target? *Curr Pharm Des* **21**, 389-416 (2015).
39. Kumar, P., Henikoff, S. & Ng, P.C. Predicting the effects of coding non-synonymous variants on protein function using the SIFT algorithm. *Nat Protoc* **4**, 1073-81 (2009).
40. Mathe, E. *et al.* Computational approaches for predicting the biological effect of p53 missense mutations: a comparison of three sequence analysis based methods. *Nucleic Acids Res* **34**, 1317-25 (2006).
41. Tavtigian, S.V. *et al.* Comprehensive statistical study of 452 BRCA1 missense substitutions with classification of eight recurrent substitutions as neutral. *J Med Genet* **43**, 295-305 (2006).
42. Bakshi, A. *et al.* Fast set-based association analysis using summary data from GWAS identifies novel gene loci for human complex traits. *Sci Rep* **6**, 32894 (2016).
43. Ferreira, M.A. *et al.* Gene-based analysis of regulatory variants identifies 4 putative novel asthma risk genes related to nucleotide synthesis and signaling. *J Allergy Clin Immunol* (2016).
44. Pickrell, J.K. Joint analysis of functional genomic data and genome-wide association studies of 18 human traits. *Am J Hum Genet* **94**, 559-73 (2014).
45. International Schizophrenia, C. *et al.* Common polygenic variation contributes to risk of schizophrenia and bipolar disorder. *Nature* **460**, 748-52 (2009).
46. Verhoeven, V.J. *et al.* Large scale international replication and meta-analysis study confirms association of the 15q14 locus with myopia. The CREAM consortium. *Hum Genet* **131**, 1467-80 (2012).
47. Finucane, H.K. *et al.* Partitioning heritability by functional annotation using genome-wide association summary statistics. *Nat Genet* **47**, 1228-35 (2015).
48. Brown, B.C., Asian Genetic Epidemiology Network Type 2 Diabetes, C., Ye, C.J., Price, A.L. & Zaitlen, N. Transethnic Genetic-Correlation Estimates from Summary Statistics. *Am J Hum Genet* **99**, 76-88 (2016).

49. Pers, T.H. *et al.* Biological interpretation of genome-wide association studies using predicted gene functions. *Nat Commun* **6**, 5890 (2015).
50. Fritsche, L.G. *et al.* A large genome-wide association study of age-related macular degeneration highlights contributions of rare and common variants. *Nat Genet* **48**, 134-43 (2016).
51. Ritchey, E.R. *et al.* Vision-guided ocular growth in a mutant chicken model with diminished visual acuity. *Exp Eye Res* **102**, 59-69 (2012).
52. Vincent, A. *et al.* Biallelic Mutations in GNB3 Cause a Unique Form of Autosomal-Recessive Congenital Stationary Night Blindness. *Am J Hum Genet* **98**, 1011-9 (2016).
53. Blake, J.A. *et al.* Mouse Genome Database (MGD)-2017: community knowledge resource for the laboratory mouse. *Nucleic Acids Res* **45**, D723-D729 (2017).
54. Nikonov, S.S. *et al.* Cones respond to light in the absence of transducin beta subunit. *J Neurosci* **33**, 5182-94 (2013).
55. Stone, E.M. *et al.* A single EFEMP1 mutation associated with both Malattia Leventinese and Doyne honeycomb retinal dystrophy. *Nat Genet* **22**, 199-202 (1999).
56. Mackay, D.S., Bennett, T.M. & Shiels, A. Exome Sequencing Identifies a Missense Variant in EFEMP1 Co-Segregating in a Family with Autosomal Dominant Primary Open-Angle Glaucoma. *PLoS One* **10**, e0132529 (2015).
57. Springelkamp, H. *et al.* ARHGEF12 influences the risk of glaucoma by increasing intraocular pressure. *Hum Mol Genet* **24**, 2689-99 (2015).
58. Haeseleer, F. *et al.* Essential role of Ca2+-binding protein 4, a Cav1.4 channel regulator, in photoreceptor synaptic function. *Nat Neurosci* **7**, 1079-87 (2004).
59. Littink, K.W. *et al.* A novel homozygous nonsense mutation in CABP4 causes congenital cone-rod synaptic disorder. *Invest Ophthalmol Vis Sci* **50**, 2344-50 (2009).
60. Grimes, W.N., Li, W., Chavez, A.E. & Diamond, J.S. BK channels modulate pre- and postsynaptic signaling at reciprocal synapses in retina. *Nat Neurosci* **12**, 585-92 (2009).
61. Parker, R.O. & Crouch, R.K. Retinol dehydrogenases (RDHs) in the visual cycle. *Exp Eye Res* **91**, 788-92 (2010).
62. Radu, R.A. *et al.* Retinal pigment epithelium-retinal G protein receptor-opsin mediates light-dependent translocation of all-trans-retinyl esters for synthesis of visual chromophore in retinal pigment epithelial cells. *J Biol Chem* **283**, 19730-8 (2008).
63. Luo, T., Sakai, Y., Wagner, E. & Drager, U.C. Retinoids, eye development, and maturation of visual function. *J Neurobiol* **66**, 677-86 (2006).
64. Keckeis, S., Reichhart, N., Roubeix, C. & Strauss, O. Anoctamin2 (TMEM16B) forms the Ca2+-activated Cl- channel in the retinal pigment epithelium. *Exp Eye Res* **154**, 139-150 (2016).
65. Prasanna, G., Narayan, S., Krishnamoorthy, R.R. & Yorio, T. Eyeing endothelins: a cellular perspective. *Mol Cell Biochem* **253**, 71-88 (2003).
66. Yamashita, T. *et al.* Essential and synergistic roles of RP1 and RP1L1 in rod photoreceptor axoneme and retinitis pigmentosa. *J Neurosci* **29**, 9748-60 (2009).
67. Davidson, A.E. *et al.* RP1L1 variants are associated with a spectrum of inherited retinal diseases including retinitis pigmentosa and occult macular dystrophy. *Hum Mutat* **34**, 506-14 (2013).
68. Hawthorne, F. *et al.* Association mapping of the high-grade myopia MYP3 locus reveals novel candidates UHRF1BP1L, PTPRR, and PPFIA2. *Invest Ophthalmol Vis Sci* **54**, 2076-86 (2013).
69. Feldkaemper, M. & Schaeffel, F. An updated view on the role of dopamine in myopia. *Exp Eye Res* **114**, 106-19 (2013).
70. Paul, M.L., Graybiel, A.M., David, J.C. & Robertson, H.A. D1-like and D2-like dopamine receptors synergistically activate rotation and c-fos expression in the dopamine-depleted striatum in a rat model of Parkinson's disease. *J Neurosci* **12**, 3729-42 (1992).
71. Stone, R.A., Lin, T., Laties, A.M. & Iuvone, P.M. Retinal dopamine and form-deprivation myopia. *Proc Natl Acad Sci U S A* **86**, 704-6 (1989).

72. Gardner, M., Bertranpetit, J. & Comas, D. Worldwide genetic variation in dopamine and serotonin pathway genes: implications for association studies. *Am J Med Genet B Neuropsychiatr Genet* **147B**, 1070-5 (2008).
73. D'Souza, U.M. & Craig, I.W. Functional polymorphisms in dopamine and serotonin pathway genes. *Hum Mutat* **27**, 1-13 (2006).
74. Beaulieu, J.M. & Gainetdinov, R.R. The physiology, signaling, and pharmacology of dopamine receptors. *Pharmacol Rev* **63**, 182-217 (2011).
75. MacArthur, J. *et al.* The new NHGRI-EBI Catalog of published genome-wide association studies (GWAS Catalog). *Nucleic Acids Res* **45**, D896-D901 (2017).
76. Holden, B.A. *et al.* Global Prevalence of Myopia and High Myopia and Temporal Trends from 2000 through 2050. *Ophthalmology* **123**, 1036-42 (2016).
77. Cardon, L.R. & Palmer, L.J. Population stratification and spurious allelic association. *Lancet* **361**, 598-604 (2003).
78. Chua, S.Y. *et al.* Age of onset of myopia predicts risk of high myopia in later childhood in myopic Singapore children. *Ophthalmic Physiol Opt* **36**, 388-94 (2016).
79. Williams, K.M. *et al.* Age of myopia onset in a British population-based twin cohort. *Ophthalmic Physiol Opt* **33**, 339-45 (2013).
80. Dolgin, E. The myopia boom. *Nature* **519**, 276-8 (2015).
81. Connaughton, V. Glutamate and Glutamate Receptors in the Vertebrate Retina. in *Webvision: The Organization of the Retina and Visual System* (eds. Kolb, H., Fernandez, E. & Nelson, R.) (Salt Lake City (UT), 1995).
82. Hung, G.K., Mahadas, K. & Mohammad, F. Eye growth and myopia development: Unifying theory and Matlab model. *Comput Biol Med* **70**, 106-18 (2016).
83. Norton, T.T. What Do Animal Studies Tell Us about the Mechanism of Myopia-Protection by Light? *Optom Vis Sci* **93**, 1049-51 (2016).
84. Weiss, S. & Schaeffel, F. Diurnal growth rhythms in the chicken eye: relation to myopia development and retinal dopamine levels. *J Comp Physiol A* **172**, 263-70 (1993).
85. Stone, R.A., Lin, T., Iuvone, P.M. & Laties, A.M. Postnatal control of ocular growth: dopaminergic mechanisms. *Ciba Found Symp* **155**, 45-57; discussion 57-62 (1990).
86. Morgan, I.G. The biological basis of myopic refractive error. *Clin Exp Optom* **86**, 276-88 (2003).
87. Li, X.X., Schaeffel, F., Kohler, K. & Zrenner, E. Dose-dependent effects of 6-hydroxy dopamine on deprivation myopia, electroretinograms, and dopaminergic amacrine cells in chickens. *Vis Neurosci* **9**, 483-92 (1992).
88. Iuvone, P.M., Tigges, M., Stone, R.A., Lambert, S. & Laties, A.M. Effects of apomorphine, a dopamine receptor agonist, on ocular refraction and axial elongation in a primate model of myopia. *Invest Ophthalmol Vis Sci* **32**, 1674-7 (1991).
89. Ashby, R., McCarthy, C.S., Maleszka, R., Megaw, P. & Morgan, I.G. A muscarinic cholinergic antagonist and a dopamine agonist rapidly increase ZENK mRNA expression in the form-deprived chicken retina. *Exp Eye Res* **85**, 15-22 (2007).
90. Ashby, R. Animal Studies and the Mechanism of Myopia-Protection by Light? *Optom Vis Sci* **93**, 1052-4 (2016).
91. Rymer, J. & Wildsoet, C.F. The role of the retinal pigment epithelium in eye growth regulation and myopia: a review. *Vis Neurosci* **22**, 251-61 (2005).
92. Chen, S. *et al.* Bright Light Suppresses Form-Deprivation Myopia Development With Activation of Dopamine D1 Receptor Signaling in the ON Pathway in Retina. *Invest Ophthalmol Vis Sci* **58**, 2306-2316 (2017).
93. Chen, P.S. *et al.* Effects of C825T polymorphism of the GNB3 gene on availability of dopamine transporter in healthy volunteers--a SPECT study. *Neuroimage* **56**, 1526-30 (2011).
94. Scott, M.S. & Ono, M. From snoRNA to miRNA: Dual function regulatory non-coding RNAs. *Biochimie* **93**, 1987-92 (2011).

95. McFadden, S.A. Understanding and Treating Myopia: What More We Need to Know and Future Research Priorities. *Optom Vis Sci* **93**, 1061-3 (2016).
96. Smith, E.L., 3rd, Hung, L.F. & Arumugam, B. Visual regulation of refractive development: insights from animal studies. *Eye (Lond)* **28**, 180-8 (2014).
97. Zhang, Y. & Wildsoet, C.F. RPE and Choroid Mechanisms Underlying Ocular Growth and Myopia. *Prog Mol Biol Transl Sci* **134**, 221-40 (2015).
98. Harper, A.R. & Summers, J.A. The dynamic sclera: extracellular matrix remodeling in normal ocular growth and myopia development. *Exp Eye Res* **133**, 100-11 (2015).
99. Summers, J.A. The choroid as a sclera growth regulator. *Exp Eye Res* (2013).
100. Howie, B., Fuchsberger, C., Stephens, M., Marchini, J. & Abecasis, G.R. Fast and accurate genotype imputation in genome-wide association studies through pre-phasing. *Nat Genet* **44**, 955-9 (2012).
101. Marchini, J., Howie, B., Myers, S., McVean, G. & Donnelly, P. A new multipoint method for genome-wide association studies by imputation of genotypes. *Nat Genet* **39**, 906-13 (2007).
102. van Leeuwen, E.M. *et al.* Population-specific genotype imputations using minimac or IMPUTE2. *Nat Protoc* **10**, 1285-96 (2015).
103. Aulchenko, Y.S., Struchalin, M.V. & van Duijn, C.M. ProbABEL package for genome-wide association analysis of imputed data. *BMC Bioinformatics* **11**, 134 (2010).
104. Chen, W.M. & Abecasis, G.R. Family-based association tests for genomewide association scans. *Am J Hum Genet* **81**, 913-26 (2007).
105. Winkler, T.W. *et al.* Quality control and conduct of genome-wide association meta-analyses. *Nat Protoc* **9**, 1192-212 (2014).
106. Willer, C.J., Li, Y. & Abecasis, G.R. METAL: fast and efficient meta-analysis of genomewide association scans. *Bioinformatics* **26**, 2190-1 (2010).
107. Zaykin, D.V. Optimally weighted Z-test is a powerful method for combining probabilities in meta-analysis. *J Evol Biol* **24**, 1836-41 (2011).
108. Whitlock, M.C. Combining probability from independent tests: the weighted Z-method is superior to Fisher's approach. *J Evol Biol* **18**, 1368-73 (2005).
109. Dudbridge, F. & Gusnanto, A. Estimation of significance thresholds for genomewide association scans. *Genet Epidemiol* **32**, 227-34 (2008).
110. Pruim, R.J. *et al.* LocusZoom: regional visualization of genome-wide association scan results. *Bioinformatics* **26**, 2336-7 (2010).
111. Yang, H. & Wang, K. Genomic variant annotation and prioritization with ANNOVAR and wANNOVAR. *Nat Protoc* **10**, 1556-66 (2015).
112. Cooper, G.M. *et al.* Distribution and intensity of constraint in mammalian genomic sequence. *Genome Res* **15**, 901-13 (2005).
113. Schwarz, J.M., Rodelsperger, C., Schuelke, M. & Seelow, D. MutationTaster evaluates disease-causing potential of sequence alterations. *Nat Methods* **7**, 575-6 (2010).
114. Loh, P.R. *et al.* Efficient Bayesian mixed-model analysis increases association power in large cohorts. *Nat Genet* **47**, 284-90 (2015).
115. McCarthy, S. *et al.* A reference panel of 64,976 haplotypes for genotype imputation. *Nat Genet* **48**, 1279-83 (2016).
116. Consortium, G.T. Human genomics. The Genotype-Tissue Expression (GTEx) pilot analysis: multitissue gene regulation in humans. *Science* **348**, 648-60 (2015).
117. Chang, C.C. *et al.* Second-generation PLINK: rising to the challenge of larger and richer datasets. *Gigascience* **4**, 7 (2015).
118. Amberger, J., Bocchini, C.A., Scott, A.F. & Hamosh, A. McKusick's Online Mendelian Inheritance in Man (OMIM). *Nucleic Acids Res* **37**, D793-6 (2009).
119. Bauer-Mehren, A., Rautschka, M., Sanz, F. & Furlong, L.I. DisGeNET: a Cytoscape plugin to visualize, integrate, search and analyze gene-disease networks. *Bioinformatics* **26**, 2924-6 (2010).

120. Gunther, S. *et al.* SuperTarget and Matador: resources for exploring drug-target relationships. *Nucleic Acids Res* **36**, D919-22 (2008).
121. Kuhn, M. *et al.* STITCH 4: integration of protein-chemical interactions with user data. *Nucleic Acids Res* **42**, D401-7 (2014).
122. Wishart, D.S. *et al.* DrugBank: a comprehensive resource for in silico drug discovery and exploration. *Nucleic Acids Res* **34**, D668-72 (2006).
123. Whirl-Carrillo, M. *et al.* Pharmacogenomics knowledge for personalized medicine. *Clin Pharmacol Ther* **92**, 414-7 (2012).

Figure 1. GWAS meta-analysis identifies 140 loci for refractive error (Stage 3)

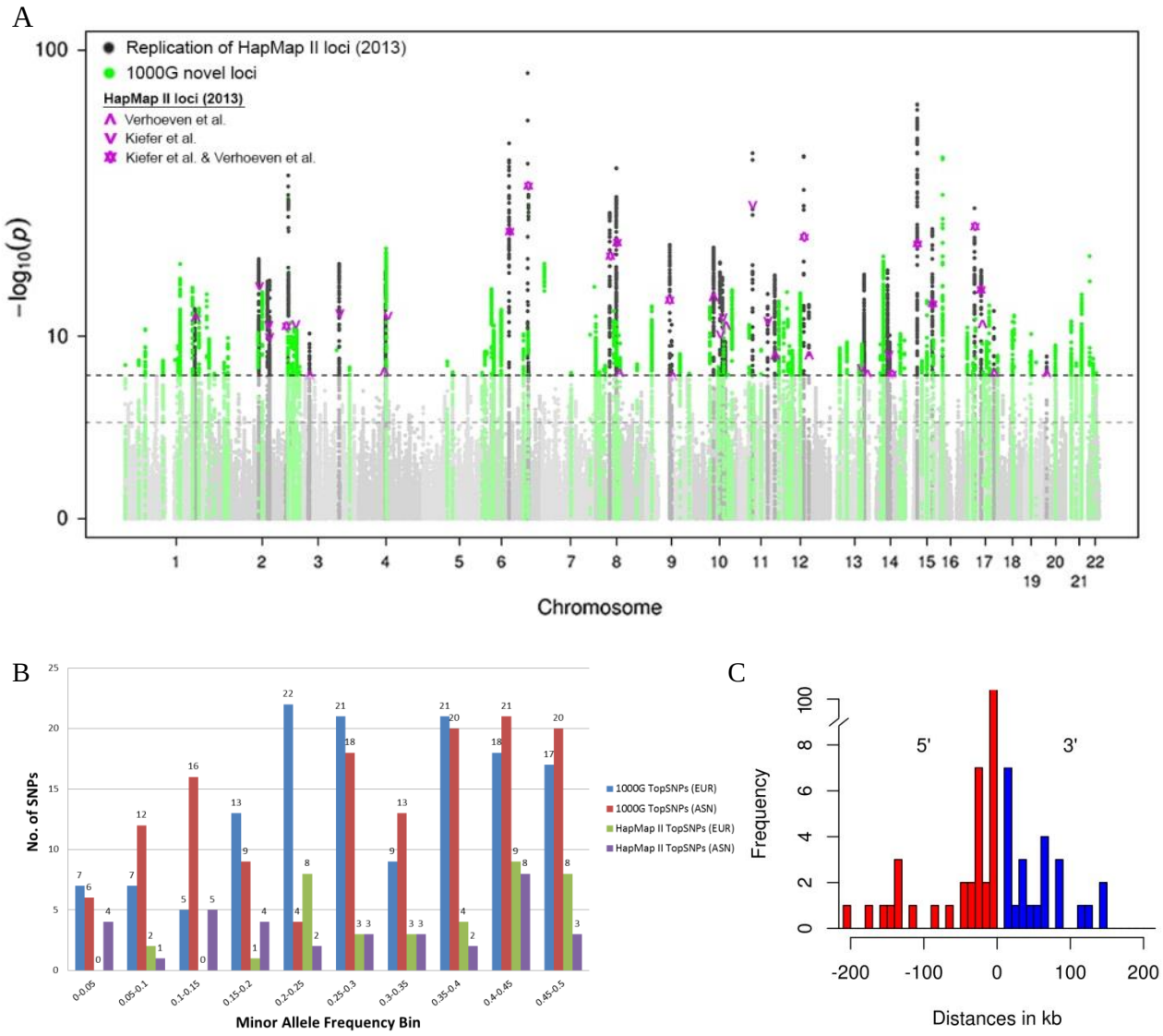

(a) We conducted a meta-analysis of genome-wide single-variant analyses for >10 million variants in 160,420 participants of CREAM and 23andMe (Stage 3). Shown is the Manhattan plot depicting *P* values for association, highlighting new ($P < 5 \times 10^{-8}$ for the first time; green) and known (dark grey) refractive error loci previously found using HapMap II imputations from Kiefer et al.[27] and Verhoeven et al.[26] (**Table 1**). The horizontal lines indicate suggestive significance ($P = 1 \times 10^{-5}$) or genome-wide

significance ($P = 5 \times 10^{-8}$). **(b)** We compared the minor allele frequencies of the 140 discovered index variants based on 1000G (blue: Europeans; red: Asians) to the minor allele frequencies of the previously found genetic variants based on HapMap II (green: Europeans; purple: Asians). Observed are an increase in genetic variants found across all minor allele frequency bins increase, including the lower minor allele frequency bins. **(c)** We annotated the 167 loci to genes using wANNOVAR. Shown are the distances between index variants from the nearest gene and its gene on the 5' and/or 3' site. The majority of index variants (84%) were at a distance of less than 50 kb up- or downstream from the annotated gene.

Table 1. Results of the meta-analysis of CREAM and 23andMe for the previously-identified loci and a subset of the newly-identified loci, and replication in UK Biobank

Table 1a Replication of the HapMap II index variants for refractive error per locus in the Stage 3 meta-analysis

SNP	Chr.	Position	Nearest Loci And Gene(s)	Effect Allele	Other Allele	EAF EUR	EAF ASN	Z-score	Direction	P value	HetISq	HetPVal	Sample Size (N)	HapMap II Discovery (2013)	Category (I = both GWS in Stage 1 and 2, 2=one of two cohorts (CREAM or 23andMe) GWS, 3= both not GWS in Stage 1 or 2)	P value Replication UKBB
rs10500355	16	7459347	RBFOX1	A	T	0.354	0.1334	-13.73	--	6.49E-43	9.1	2.93E-07	160139	Kiefer et al. & Verhoeven et al.	I	2.50E-48
rs11145465	9	71766593	TJP2	A	C	0.212	NA	-9.55	--	1.35E-21	46.3	0.1722	153174	Kiefer et al. & Verhoeven et al.	I	1.00E-10
rs11178469	12	71275137	PTPRR	T	C	0.752	0.6384	-7.40	--	1.33E-13	0	0.6989	160139	Verhoeven et al.	II (CREAM)	2.60E-04
rs11602008	11	40149305	LRRC4C	A	T	0.822	0.7488	13.98	++	2.12E-44	22.5	1.56E-10	157505	Kiefer et al.	II (23andMe)	2.90E-47
rs12193446	6	129820038	BC035400, LAMA2	A	G	0.906	NA	-19.43	--	4.21E-84	16.8	5.72E-15	150269	Kiefer et al. & Verhoeven et al.	I	4.60E-106
rs1550094	2	233385396	CHRNG,PRSS56	A	G	0.701	0.705	12.74	++	3.64E-37	26.3	0.002705	159422	Kiefer et al. & Verhoeven et al., Kiefer et al.	I	4.10E-59
rs1649068	10	60304864	BICC1	A	C	0.475	0.5044	-9.44	--	3.77E-21	0	0.7118	160144	Verhoeven et al.	I	7.50E-11
rs17382981	10	94953258	CYP26A1,MYOF	T	C	0.417	0.1901	-6.31	--	2.72E-10	67.9	0.07737	155332	Verhoeven et al.	II (CREAM)	4.10E-07
rs17428076	2	172851936	HAT1,METAP1D	C	G	0.768	0.8542	-8.18	--	2.77E-16	0	0.002854	160151	Kiefer et al.	II (23andMe)	7.50E-08
rs1858001	1	207488004	C4BPA,CD55	C	G	0.676	0.4151	7.28	++	3.45E-13	59.6	0.02007	160149	Verhoeven et al.	II (CREAM)	6.70E-20
rs1954761	11	105596885	GRIA4	T	C	0.371	0.3772	-8.40	--	4.57E-17	0	0.911	160122	Verhoeven et al.	I	1.20E-16
rs2155413	11	84634790	DLG2	A	C	0.482	0.6549	-7.76	--	8.85E-15	0	0.0002987	159504	Kiefer et al.	II (23andMe)	1.10E-17
rs235770	20	6761765	BMP2	T	C	0.372	0.3875	-5.93	--	3.11E-09	0	0.5474	157521	Verhoeven et al.	II (23andMe)	4.80E-11
rs2573081	2	178828507	PDE11A	C	G	0.524	0.5378	8.21	++	2.18E-16	47.6	0.1672	160126	Kiefer et al.	II (23andMe)	1.60E-29
rs2753462	14	60850703	JB175233,C14orf39	C	G	0.296	0.5679	-6.49	--	8.37E-11	73.9	0.05032	157352	Verhoeven et al.	II (CREAM)	2.00E-15
rs2855530	14	54421917	BMP4	C	G	0.507	0.4736	-8.58	--	9.87E-18	41.7	0.1904	160092	Kiefer et al.	I	4.80E-22
rs2908972	17	11407259	SHISA6	A	T	0.415	0.4879	-11.13	--	9.46E-29	23	0.2544	160123	Kiefer et al. & Verhoeven et al.	I	6.10E-29
rs3138141	12	56115778	BLOC1S1-RDH5,RDH5	A	C	0.214	0.1472	13.80	++	2.46E-43	3.2	5.05E-07	157531	Kiefer et al. & Verhoeven et al.	I	2.30E-56
rs4687586	3	53837971	CACNA1D	C	G	0.691	NA	-6.55	--	5.86E-11	0	0.6046	150217	Verhoeven et al.	III	1.60E-08
rs4793501	17	68718734	KCNJ2,BC039327	T	C	0.575	0.444	-7.21	--	5.53E-13	0	0.5917	160150	Verhoeven et al.	II (CREAM)	3.70E-12
rs524952	15	35005886	GOLGA8B,GJD2	A	T	0.475	0.5077	-17.08	--	2.28E-65	67.2	0.01544	160150	Kiefer et al. & Verhoeven et al.	I	1.60E-103
rs56075542	2	146882415	BC040861,PABPC1P2	T	G	0.552	0.4726	-8.99	--	2.39E-19	13.9	0.001284	159478	Kiefer et al.	II (23andMe)	1.30E-18
rs62070229	17	31227593	MYO1D,TMEM98	A	G	0.807	0.8747	8.58	++	9.64E-18	0	0.4158	156570	Verhoeven et al.	I	1.30E-18
rs6495367	15	79375347	RASGRF1	A	G	0.408	0.3988	-10.20	--	1.95E-24	0	0.667	160144	Kiefer et al. & Verhoeven et al.	I	7.20E-37
rs7042950	9	77149837	RORB	A	G	0.732	0.3924	6.80	++	1.07E-11	0	0.9122	160153	Verhoeven et al.	III	2.90E-18
rs72621438	8	60178580	SNORA51,CA8	C	G	0.642	0.6089	-13.14	--	2.03E-39	38.4	0.00559	160128	Kiefer et al. & Verhoeven et al.	I	1.80E-49
rs745480	10	85986554	LRIT2,LRIT1	C	G	0.511	0.4182	8.31	++	9.26E-17	67.3	0.0805	159504	Kiefer et al.	II (23andMe)	8.20E-18
rs7624084	3	141093285	ZBTB38	T	C	0.568	0.6332	-8.81	--	1.24E-18	18.5	0.01802	160151	Kiefer et al.	II (23andMe)	6.50E-17
rs7662551	4	80537638	LOC100506035,PCAT4	A	G	0.723	0.5577	8.53	++	1.47E-17	19.4	0.2653	160147	Verhoeven et al.	I	6.00E-12
rs7692381	4	81903049	C4orf22,BMP3	A	G	0.763	0.6308	9.40	++	5.55E-21	0	0.01253	160134	Kiefer et al.	I	7.50E-13
rs7744813	6	73643289	KCNQ5	A	C	0.591	0.6017	-14.56	--	5.43E-48	35	0.001132	160091	Kiefer et al. & Verhoeven et al.	I	1.00E-75
rs7829127	8	40726394	ZMAT4	A	G	0.792	0.8974	-10.91	--	1.02E-27	15.9	0.0002774	160132	Kiefer et al. & Verhoeven et al.	II (23andMe)	3.10E-22
rs7895108	10	79061458	KCNMA1	T	G	0.351	0.1182	-8.87	--	7.56E-19	32.8	0.02115	160140	Kiefer et al.	II (23andMe)	1.10E-27
rs79266634	16	7309047	RBFOX1	C	G	0.093	0.1151	-5.93	--	3.00E-09	0	0.5614	156268	Kiefer et al. & Verhoeven et al.	III	1.50E-08
rs837323	13	101175664	PCCA	T	C	0.512	0.7625	6.32	++	2.65E-10	35.6	0.2129	160142	Verhoeven et al.	II (23andMe)	5.30E-16
rs9517964	13	100717833	ZIC2,PCCA	T	C	0.589	0.786	8.42	++	3.68E-17	0	0.01962	160121	Kiefer et al.	II (23andMe)	3.40E-20

Table 1b Subset of the new loci harboring the smallest p-values for refractive error in the Stage 3 meta-analysis

SNP	Chr.	Position	Nearest Loci And Gene(s)	Effect Allele	Other Allele	EAF EUR	EAF ASN	Z-score	Direction	P value	HetISq	HetPVal	Sample Size (N)	Category (I = both GWS in Stage 1 and 2, 2=one of two cohorts (CREAM or 23andMe) GWS, 3= not GWS in Stage 1 or 2)	P value Replication UKBB
rs36024104	14	42294993	LRFN5	A	G	0.823	NA	9.09	++	9.86E-20	15.9	0.01414	152585	II (23andMe)	2.20E-12
rs7456039	7	6901710	CCZ1B,LOC100131257	C	G	0.183	NA	8.82	++	1.18E-18	42.1	3.79E-12	121337	II (23andMe)	6.50E-01
rs1556867	1	164213686	5S_rRNA,PBX1	T	C	0.264	0.494	-8.81	--	1.29E-18	71.1	0.06266	160155	II (23andMe)	4.20E-17
rs12667032	7	154406581	DPP6	A	G	0.152	0.317	7.99	++	1.31E-15	82.3	1.02E-11	130790	II (23andMe)	2.10E-01
rs2225986	1	200311910	LINC00862	A	T	0.381	0.169	-7.96	--	1.68E-15	40.2	0.196	160152	II (23andMe)	7.50E-17
rs1207782	6	22059967	LINC00340	T	C	0.577	0.265	-7.92	--	2.47E-15	0	0.8946	160149	I	4.90E-13
rs72826094	10	114801488	TCF7L2	A	T	0.799	0.838	7.88	++	3.20E-15	64.5	0.09323	156825	II (23andMe)	4.90E-02
rs297593	2	157363743	GPD2	T	C	0.286	0.257	-7.82	--	5.45E-15	0	0.5285	159461	II (23andMe)	7.80E-11
rs5442	12	6954864	GNB3	A	G	0.068	NA	-7.82	--	5.48E-15	8.8	0.03693	146217	II (23andMe)	1.20E-33
rs10880855	12	46144855	ARID2	T	C	0.507	0.464	-7.78	--	7.35E-15	0	0.9683	160144	I	4.80E-08
rs12405776	1	242431557	PLD5	T	C	0.220	0.521	7.75	++	9.52E-15	64.9	3.56E-10	153784	II (23andMe)	1.50E-01
rs2150458	21	47377296	PCBP3,COL6A1	A	G	0.455	0.641	7.74	++	1.04E-14	55.7	0.1329	160151	II (23andMe)	1.80E-13
rs12898755	15	63574641	APH1B	A	G	0.245	0.456	7.53	++	4.98E-14	7.9	0.2974	159506	II (23andMe)	1.40E-16
rs7122817	11	117657679	DSCAML1	A	G	0.507	0.662	7.51	++	5.73E-14	73.8	0.05077	160147	II (23andMe)	1.10E-10
rs10511652	9	18362865	SH3GL2,ADAMTSL1	A	G	0.416	0.445	7.36	++	1.91E-13	44.8	0.1782	160149	II (23andMe)	3.50E-18
rs11101263	10	49414181	FRMPD2	T	C	0.258	0.105	-7.33	--	2.33E-13	0	0.3477	160155	II (23andMe)	2.20E-13
rs11118367	1	219790221	LYPLAL1	T	C	0.482	0.630	-7.29	--	3.16E-13	0	0.8576	160141	III	1.20E-13
rs9395623	6	50757699	TFAP2D,TFAP2B	A	T	0.315	0.381	7.25	++	4.16E-13	0	0.9579	160151	III	2.20E-10
rs284816	8	53362145	ST18,FAM150A	A	G	0.163	0.198	-7.21	--	5.52E-13	0	0.9242	160140	III	1.60E-08
rs12965607	18	47391025	MYO5B	T	G	0.857	0.923	7.07	++	1.52E-12	20.8	0.01674	157604	II (23andMe)	8.10E-16
rs7747	4	80827062	ANTXR2	T	C	0.202	0.093	7.03	++	2.05E-12	5.4	0.01267	150327	II (23andMe)	7.70E-16
rs12451582	17	54734643	NOG,C17orf67	A	G	0.369	0.308	7.02	++	2.22E-12	0	0.5925	160155	II (23andMe)	8.80E-18
rs80253120	17	14138507	CDRT15	T	C	0.626	0.723	6.97	++	3.25E-12	58.6	0.12	156054	II (23andMe)	7.20E-11
22:23069851:I	22	23069851	DKFZp667J0810,abParts	ATG	A	0.084	0.1582	6.95	-+	3.56E-12	98.5	4.80E-16	120481	II (23andMe)	9.30E-01
rs7968679	12	9313304	PZP	A	G	0.700	0.894	6.95	++	3.65E-12	0	0.01951	160076	II (23andMe)	4.20E-10
rs11202736	10	90142203	RNLS	A	T	0.717	0.762	-6.92	--	4.53E-12	0	0.4007	160150	II (23andMe)	9.40E-07
rs11088317	21	16574122	NRIP1,USP25	T	C	0.287	0.299	-6.90	--	5.38E-12	72.5	0.05657	160116	II (23andMe)	6.50E-06
rs10853531	18	42824449	SLC14A2	A	G	0.200	0.182	6.88	++	5.89E-12	0	0.6755	160104	III	2.60E-10
rs72655575	8	60556509	SNORA51,CA8	A	C	0.201	0.124	6.87	++	6.54E-12	0	0.8811	156566	I	7.10E-07
rs12998513	2	242879499	CXXC11,AK097934	A	G	0.880	0.676	-6.86	+-	7.15E-12	65.2	4.51E-14	117611	II (23andMe)	7.80E-01
rs1790165	11	131928971	NTM	A	C	0.411	0.283	6.85	++	7.17E-12	0	0.003708	160131	II (23andMe)	1.80E-10
rs511217	11	30029948	METTL15,KCNA4	A	T	0.738	0.729	-6.79	--	1.10E-11	0	0.3626	160143	II (23andMe)	1.40E-17
rs1150687	6	28162469	ZNF192P1,TRNA_Ser	T	C	0.619	0.504	6.78	++	1.17E-11	56.2	0.131	159448	II (23andMe)	3.10E-10
rs56055503	16	80532694	MAF,DYNLRB2	A	G	0.751	0.539	-6.72	--	1.83E-11	0	0.8407	160145	II (23andMe)	8.00E-06
rs9681162	3	8194734	AK124857,LMCD1-AS1	T	C	0.680	0.437	6.70	++	2.10E-11	63	0.1002	160152	II (23andMe)	6.30E-13
rs11589487	1	61342229	AK097193,BC030753	A	G	0.445	0.089	6.67	++	2.64E-11	34.6	0.2163	160143	II (23andMe)	2.20E-10

We identified 140 loci for refractive error with genome-wide significance ($P < 5 \times 10{-}8$) on the basis the meta-analyses of the genome-wide single-variant linear regressions performed in 160,420 participants of mixed ancestries (CREAM-ASN, CREAM-EUR and 23andMe). Shown are the replication of the previously found loci from HapMap II and a subset of the new loci harboring the smallest p-values. For each locus, represented by an index variant (the variant with smallest p-value in that locus), Effect Allele, Other Allele, effect allele frequencies per ancestry (EAF AZN and EAF EUR), effect size (Z-score), direction of the effect (Direction), the P value, heterogeneity I square (HetISq), heterogeneity P value (HetPval), Sample Size (N), Category and P value of the replication in UK Biobank are shown (Full table: Supplementary Excel Table 1). Chr., chromosome; EAF, effect allele frequency; ASN, Asian; EUR, European; GWS, genome wide significant; UKBB, United Kingdom Biobank.

Figure 2. Correlation of statistical significance and effect size of SNPs based on spherical equivalent (SphE) in diopters and age of diagnosis of myopia (AODM) in years.

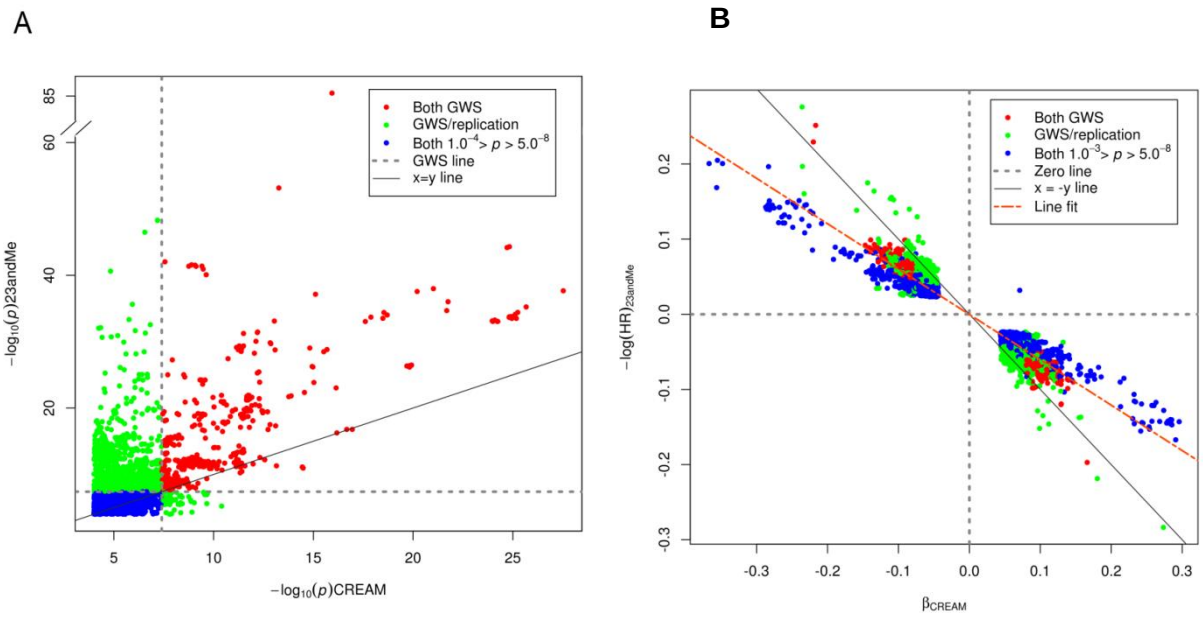

(a) *P* value per genetic variant comparison between CREAM meta-analysis (Stage 1) and 23andMe (Stage 2) meta-analysis. Shown is the overlap (red) and the difference (green) in *P* value signals per cohort for genetic variants. Green genetic variants are only genome wide significant in either CREAM or 23andMe. Blue: genetic variants with P value between 5.0×10^{-8} and 1.0×10^{-3} in both CREAM and 23andMe. **(b)** Comparison of effects (SphE and logHR of AODM in years) between CREAM and 23andMe. Same color code was applied as in (a). The effects were concordant in their direction of effect on refractive error. The regression slope is -0.15 diopters per logHR of AODM in years.

Figure 3. Risk of refractive error per decile of polygenic risk score (Rotterdam Study I-III, N = 10,792)

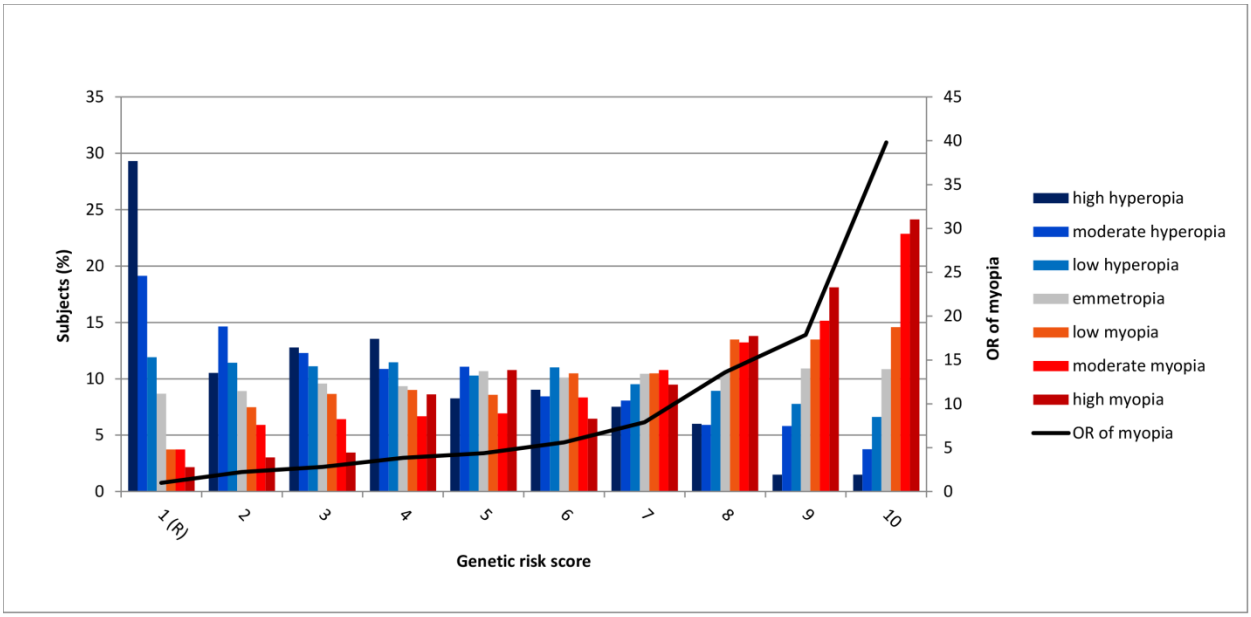

Distribution of refractive error in subjects from Rotterdam Study I–III (*N* = 10,792) as a function of the optimal polygenic risk score (including 7,303 variants at *P* value ≤ 0.005 explaining 7.8% of the variance of SphE; Supplementary Table 9). Mean OR of myopia (black line) was calculated per polygenic risk score category using the lowest category as a reference. High myopia (SphE ≤-6 D), moderate myopia (SphE >-6 D & ≤ −3 D), low myopia (SphE > −3 D & <-1.5 D), emmetropia (SphE ≥ −1.5 D and ≤ 1.5 D), low hyperopia (SphE > 1.5 D & < 3 D), moderate hyperopia (SphE ≥ 3 D & 6 D), high hyperopia (SphE ≥ 6 D).

Table 1. Genetic correlation for refractive error between Europeans and East Asians

Sample 1	Sample 2	Genetic effect correlation (*pge*) [a]	Genetic impact correlation (*pgi*) [a]
EUR CREAM	**EAS CREAM**	**0.804 (se=0.041) $P = 1.83 \times 10^{-6}$**	**0.888 (se=0.061) $P = 0.065$**
EUR 23andMe	**EAS CREAM**	**0.788 (se=0.041) $P = 2.48 \times 10^{-7}$**	**0.865 (se=0.054) $P = 0.014$**
Abbreviations: EUR, European; EAS, East Asian.			
[a] P-value relates to a test of the null hypothesis that *pge*=1 or *pgi*=1.			

We calculated the genetic correlation of effect (pge) and impact (pgi) using Popcorn to compare the genetic associations between Europeans (CREAM-EUR, N= 44,192; 23andMe, N=104,292) and East Asians (CREAM-ASN, N= 9,826). Reference panels for Popcorn were constructed using genotype data for 503 EUR and 504 EAS individuals sequenced as part of the 1000 Genomes Project. SNPs used had a MAF of at least 5% in both populations, resulting in a final set of 3,625,602SNPs for the analyses using the 23andMe GWAS sample and 3,642,928 SNPs for those using the CREAM-EUR sample. These findings support a largely common genetic predisposition to refractive error and myopia in Europeans and Asians, although ancestry-specific risk alleles may exist.

Figure 4. Visualization of the DEPICT gene-set enrichment analysis based on loci associated with refractive error and the correlation between the (meta)gene sets

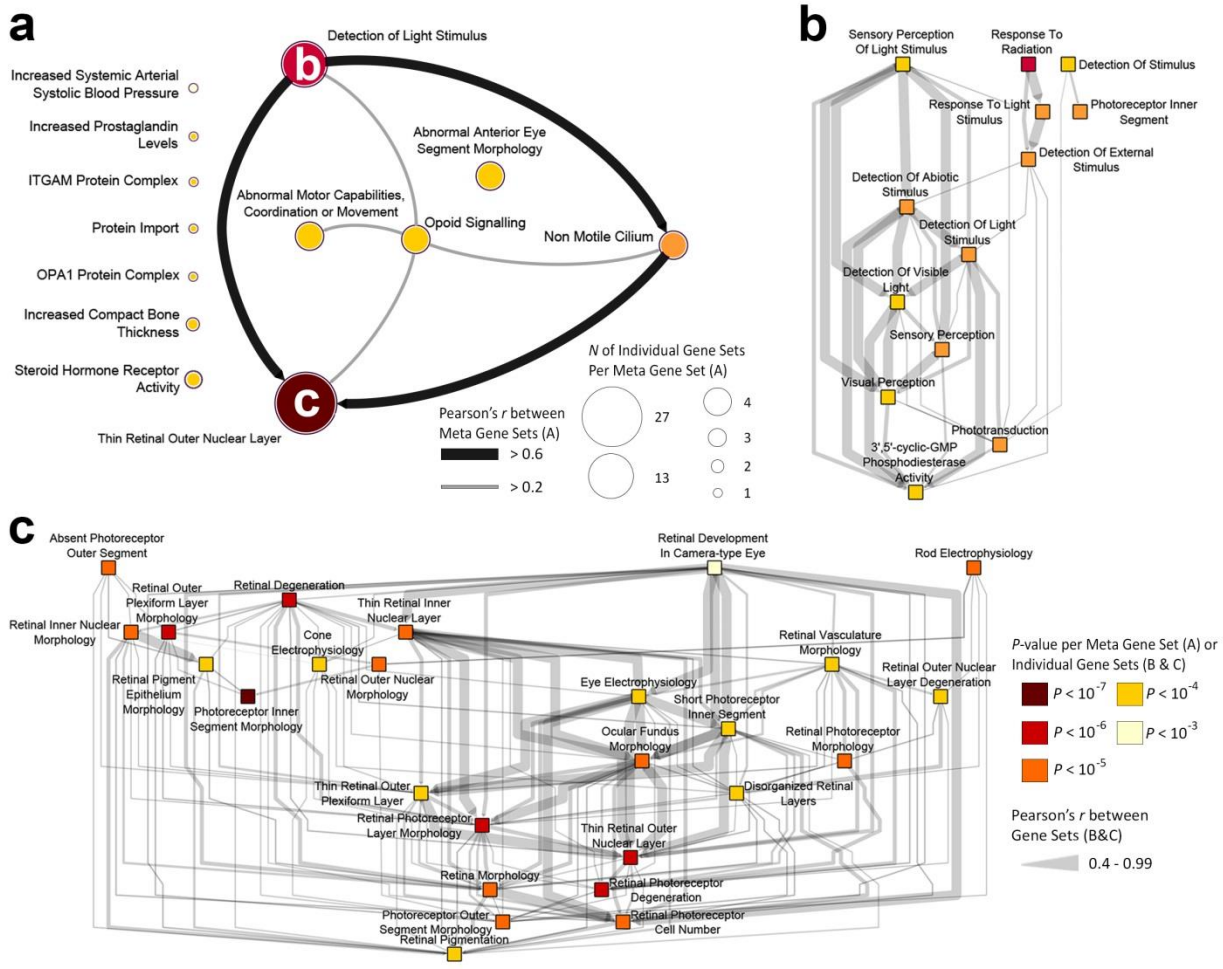

(a) Shown are the 66 gene sets clustered into thirteen meta gene sets based on the gene set enrichment analysis of DEPICT (*P* value < 1 × 10−5 in the GWAS, FDR < 0.05). **(b)** Visualization of the interconnectivity between gene sets (n=13) of the meta gene set 'Detection of Light Stimulus' (GO:0009583). **(c)** Visualization of the interconnectivity between gene sets (n=27) of the largest meta gene set 'Thin Retinal Outer Nuclear Layer' (MP:0008515). In all panels, (meta)gene sets are represented by nodes colored according to statistical significance, and similarities between them are indicated by edges scaled according to their correlation; r ≥ 0.2 are shown in panel **(a)** and r ≥ 0.4 are shown in panel **(b,c).**

Table 2. Genes ranked according to biological and statistical evidence

			ANNOTATION*				EXPRESSION			BIOLOGY		PATHWAYS				
Score	Σ	1	1	1	1	1	1	1	1	1	1	1	1	1		
Locus	Gene Priority Score	Internal Replication (≥2 cohorts)	Exonic: Protein Altering	Exonic: Non-Protein Altering	5'or 3' UTR	RNA (nc, sno, linc, other)	eQTL	Expression in human adult ocular tissue	Expression in human developing ocular tissue (fetal - 24 weeks)	Ocular phenotype in mice	Ocular phenotype in human	DEPICT gene-set enrichment	DEPICT gene prioritization	IPA Canonical Pathways		Known Drug Target
GNB3	8															
RDH5	7															
CYP26A1	7															
EFEMP1	7															
GRIA4	7															
RGR	7															
RORB	7															
RCBTB1	6															
MAF	6															
ZEB2	6															
KCNMA1	6															
TJP2	6															
ST18	6															
FBN1	6															
KCNJ2	6															
GJD2	6															
CABP4	6															
TCF7L2	6															
PRSS56	6															

Genes were ranked (orange) based on 10 equal categories which can be divided in four categories: internal replication of genetic variant in more than two cohorts (purple; CREAM-EUR, CREAM-ASN and/or 23andMe), annotation (light blue; genetic variant harboring an exonic protein altering variant or non-protein altering variant, genetic variant residing in a 5' or 3' UTR region of a gene or transcribing an RNA structure), expression (yellow; eQTL, expression in adult human ocular tissue, expression in developing ocular tissue), biology (dark yellow; ocular phenotype in mice, ocular phenotype in humans), pathways (green; DEPICT gene-set enrichtment, DEPICT gene prioritization analysis and canonical pathway analysis of IPA). We assessed genes harboring drug targets (salmon red), but did not assign a scoring point to this category.

*Only one point can be assigned in the category 'ANNOTATION', even though it has four columns (i.e. a genetic variant is located in only 1 of these four categories).

Figure 5. Top molecular network identified by Ingenuity Pathway Analysis (IPA)

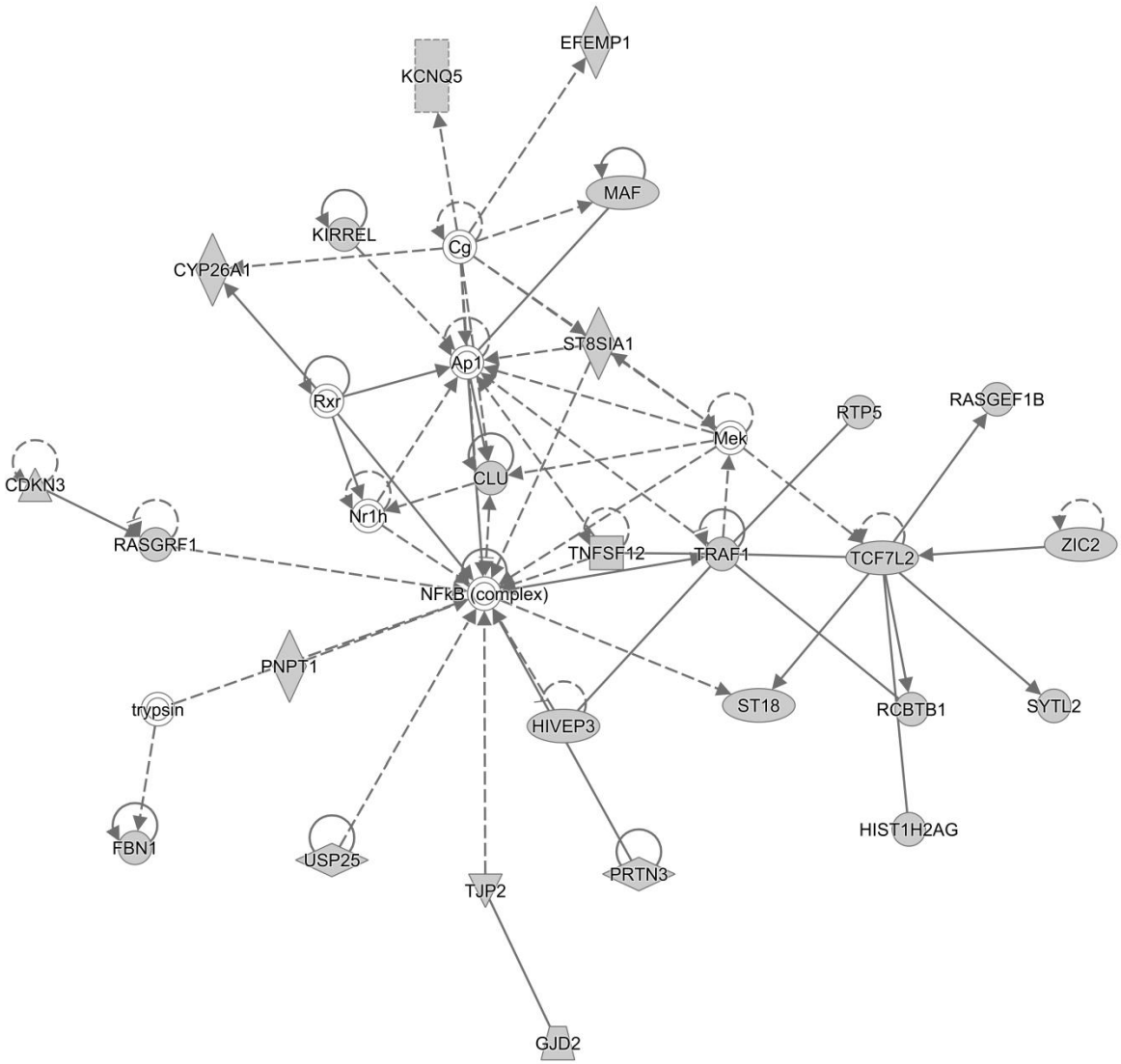

The genes annotated to the top hits identified at Stage 3 were mapped to networks and pathways present in the IPA database. The most significant network identified by Fisher's exact test was 'Glutamate Receptor Signaling' (*P* value= 1.56×10^{-4}). Genes within the network indicated in grey are genes associated with refractive error. Other significant pathways are depicted in Supplementary Figure 10.

Figure 6. Schematic representation of the human eye, retinal cell types, and functional sites of associated genes

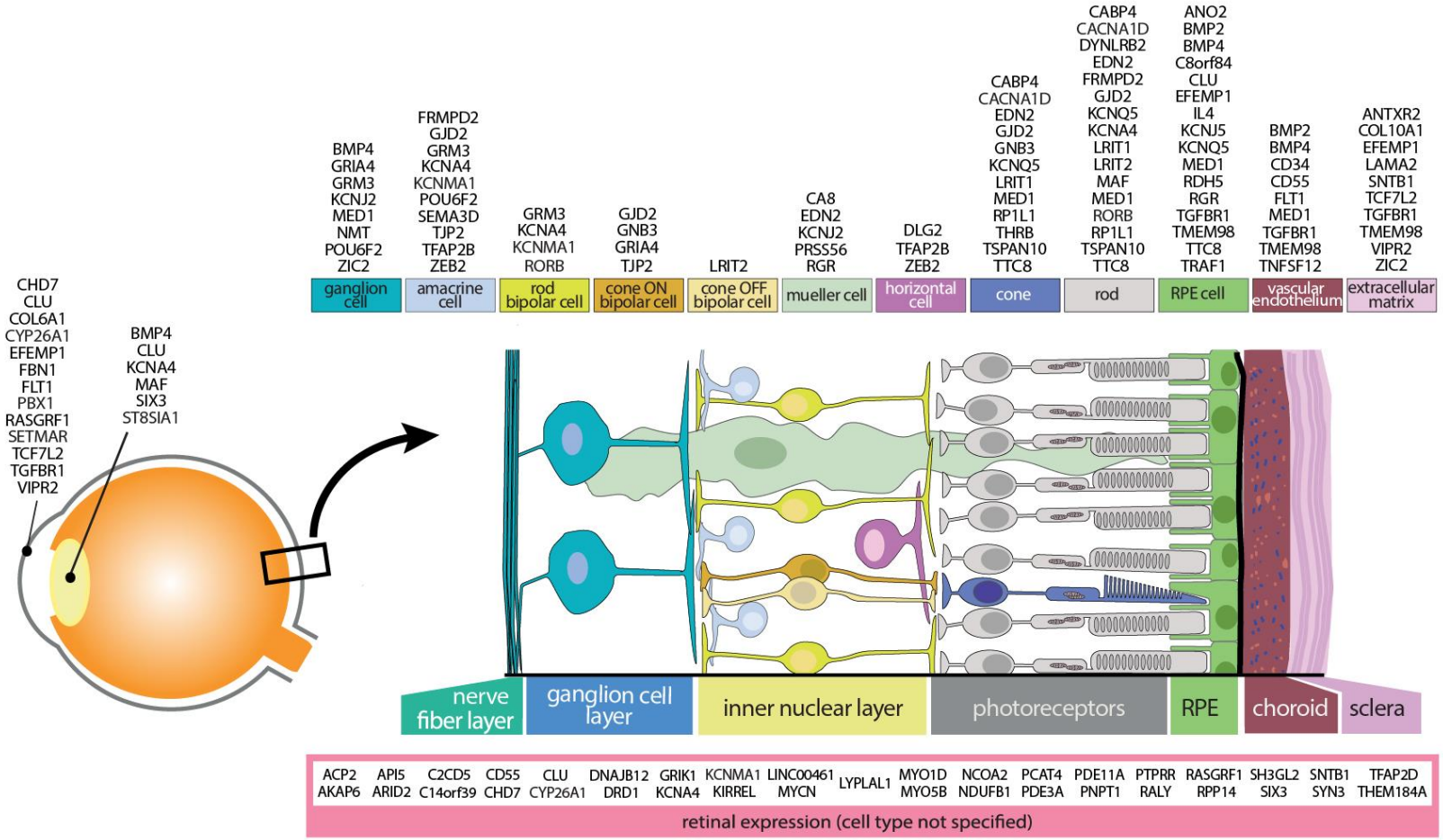

We assessed gene expression sites and/or functional target cells in the eye for all genes using our expression data and literature and data present in the public domain. The genes appear to be distributed across virtually all cell types in the neurosensory retina, in the RPE, vascular endothelium and extracellular matrix; i.e., the route of the myopic retina-to-sclera signalling cascade.

The CREAM Consortium

Tin Aung[1,2], Joan E. Bailey-Wilson[3], Paul Nigel Baird[4], Amutha Barathi Veluchamy[1,5], Ginevra Biino[6], Kathryn P. Burdon[7], Harry Campbell[8], Li Jia Chen[9], Peng Chen[2], Wei Chen[10], Ching-Yu Cheng[1,2,5], Emily Chew[11], Jamie E. Craig[7], Phillippa Cumberland[12,13], Margaret M. Deangelis[14], Cécile Delcourt[15,16], Xiaohu Ding[17], Angela Döring[18], Cornelia M. van Duijn[19], David M. Evans[20,21], Qiao Fan[22], Lindsay Farrer[14], Sheng Feng[23], Brian Fleck[24], Rhys D. Fogarty[7], Jeremy R. Fondran[25], Maurizio Fossarello[26], Paul J. Foster[27,28], Puya Gharahkhani[29], Christian Gieger[18], Adriana I. Iglesias Gonzalez[19,30],, Jeremy A. Guggenheim[31], Xiaobo Guo[17,32], Toomas Haller[33], Christopher J. Hammond[34,35], Caroline Hayward[36], Mingguang He[4,17], Alex W. Hewitt[4,37], René Höhn[38], S. Mohsen Hosseini[39], Laura D. Howe[20,40], Pirro G Hysi[35], Robert P. Igo Jr[25], Sudha K. Iyengar[11,25,41], Sarayut Janmahasatian[25], Vishal Jhanji[9], Jost B. Jonas[42-44], Mika Kähönen[45], Jaakko Kaprio[46], John P. Kemp[20], Kay-Tee Khaw[47], Anthony P. Khawaja[47], Chiea-Chuen Khor[2,48-50], Caroline C. W. Klaver[19,30], Barbara E. Klein[51], Ronald Klein[51], Eva Krapohl[52], Jean-François Korobelnik[15,16], Jonathan H. Lass[25,41], Elisabeth M. van Leeuwen[19,30], Terho Lehtimäki[53], Yi Lu[29], Robert N. Luben[47], Stuart MacGregor[29], David A. Mackey[4,37], Kari-Matti Mäkelä[53], Nicholas G. Martin[54], George McMahon[20], Akira Meguro[55], Thomas Meitinger[56], Andres Metspalu[33], Evelin Mihailov[33], Paul Mitchell[57], Masahiro Miyake[58], Nobuhisa Mizuki[55], Margaux Morrison[14], Vinay Nangia[59],Songhomitra Panda-Jonas[59], Chi Pui Pang[9], Olavi Pärssinen[60,61], Andrew D. Paterson[39], Norbert Pfeiffer[38], Mario Pirastu[62], Robert Plomin[52], Ozren Polasek[8,63], Jugnoo S. Rahi[12,13,64], Olli Raitakari[65,66], Taina Rantanen[60,67], Janina S. Ried[18], Igor Rudan[8], Seang-Mei Saw[1,48], Maria Schache[4], Ilkka Seppälä[53], George Davey Smith[20], Dwight Stambolian[68], Beate St Pourcain[20,69], Claire L. Simpson[3,70], E-Shyong Tai[5,48,71], Pancy O. Tam[9], Milly S. Tedja[19,30], Yik-Ying Teo[48,72], J. Willem L. Tideman[19,30], Nicholas J. Timpson[20], Simona Vaccargiu[62], Zoran Vatavuk[73], Virginie J.M. Verhoeven[19,30], Veronique Vitart[36], Jie Jin Wang[4,57], Nick J. Wareham[74], Juho Wedenoja[46,75], Cathy Williams[40], Katie M Williams[34,35], James F. Wilson[8], Robert Wojciechowski[3,76,77], Ya Xing Wang[42,43], Tien-Yin Wong[1,2], Alan F. Wright[36], Jing Xie[4],

Liang Xu[42], Kenji Yamashiro[58], Maurice K.H. Yap[78], Seyhan Yazar[37], Shea Ping Yip[79], Nagahisa Yoshimura[58], Alvin L. Young[9], Terri L. Young[5,51], Jing Hua Zhao[74], Wanting Zhao[1], Xiangtian Zhou[10]

1. Singapore Eye Research Institute, Singapore National Eye Centre, Singapore, Singapore.
2. Department of Ophthalmology, National University Health Systems, National University of Singapore, Singapore.
3. Computational and Statistical Genomics Branch, National Human Genome Research Institute, National Institutes of Health, Baltimore, MD, USA.
4. Centre for Eye Research Australia (CERA), Ophthalmology, Department of Surgery, University of Melbourne, Royal Victorian Eye and Ear Hospital, Melbourne, Victoria, Australia.
5. Duke-NUS Medical School, Singapore, Singapore.
6. Institute of Molecular Genetics, National Research Council, Pavia, Italy.
7. Department of Ophthalmology, Flinders University, Adelaide, Australia.
8. Centre for Global Health Research, The Usher Institute for Population Health Sciences and Informatics, University of Edinburgh, Scotland, UK.
9. Department of Ophthalmology and Visual Sciences, The Chinese University of Hong Kong Hong Kong Eye Hospital, Kowloon, Hong Kong.
10. Department of Radiology, Southwest Hospital, The Third Military Medical University, Chongqing, China.
11. Department of Genetics, Case Western Reserve University, Cleveland, Ohio, USA.
12. Institute of Child Health, University College London, London, UK.
13. Ulverscroft Vision Research Group, University College London, London, UK.
14. Department of Ophthalmology and Visual Sciences, John Moran Eye Center, University of Utah, Salt Lake City, Utah, USA.
15. Université de Bordeaux, Bordeaux, France.
16. INSERM (Institut National de la Santé Et de la Recherche Médicale), ISPED (Institut de Santé Publique d'Épidémiologie et de Développement), Centre INSERM U897-Epidemiologie-Biostatistique, Bordeaux, France.
17. State Key Laboratory of Ophthalmology, Zhongshan Ophthalmic Center, Sun Yat-sen University, Guangzhou, China.
18. Institute of Genetic Epidemiology, Helmholtz Zentrum München—German Research Center for Environmental Health, Neuherberg, Germany.
19. Department of Epidemiology, Erasmus Medical Center, Rotterdam, The Netherlands.
20. MRC Integrative Epidemiology Unit (IEU) at the University of Bristol, Bristol, UK.
21. University of Queensland Diamantina Institute, Translational Research Institute, Brisbane, Queensland, Australia.
22. Centre for Quantitative Medicine, Duke-NUS Medical School, Singapore, Singapore.
23. Department of Pediatric Ophthalmology, Duke Eye Center For Human Genetics, Durham, North Carolina, USA.
24. Princess Alexandra Eye Pavilion, Edinburgh, UK.
25. Department of Epidemiology and Biostatistics, Case Western Reserve University, Cleveland, Ohio, USA.
26. University Hospital 'San Giovanni di Dio', Cagliari, Italy.
27. Division of Genetics and Epidemiology, UCL Institute of Ophthalmology, London, UK.
28. NIHR Biomedical Research Centre, Moorfields Eye Hospital NHS Foundation Trust and UCL Institute of Ophthalmology, London, UK.
29. Statistical Genetics Laboratory, QIMR Berghofer Medical Research Institute, Herston, Brisbane, Queensland, Australia.

30. Department of Ophthalmology, Erasmus Medical Center, Rotterdam, The Netherlands.
31. School of Optometry & Vision Sciences, Cardiff University, Cardiff, UK.
32. Department of Statistical Science, School of Mathematics & Computational Science, Sun Yat-Sen University, Guangzhou.
33. Estonian Genome Center, University of Tartu, Tartu, Estonia.
34. Department of Ophthalmology, King's College London, St Thomas' Hospital campus, London, UK.
35. Department of Twin Research and Genetic Epidemiology, King's College London School of Medicine, London, UK.
36. Medical Research Council Human Genetics Unit, Institute of Genetics and Molecular Medicine, University of Edinburgh, Edinburgh, UK.
37. Centre for Ophthalmology and Visual Science, Lions Eye Institute, University of Western Australia, Perth, Australia.
38. Department of Ophthalmology, University Medical Center Mainz, Mainz, Germany.
39. Genetics and Genome Biology Program, Hospital for Sick Children and University of Toronto, Toronto, Ontario, Canada.
40. School of Social and Community Medicine, University of Bristol, Bristol, UK.
41. Department of Ophthalmology and Visual Sciences, Case Western Reserve University and University Hospitals Eye Institute, Cleveland, Ohio, USA.
42. Beijing Institute of Ophthalmology, Beijing Tongren Hospital, Capital Medical University, Beijing, China.
43. Beijing Ophthalmology and Visual Science Key Lab, Beijing, China.
44. Department of Ophthalmology, Medical Faculty Mannheim, Ruprecht-Karls-University Heidelberg, Mannheim, Germany.
45. Department of Clinical Physiology, Tampere University Hospital and School of Medicine, University of Tampere, Tampere, Finland.
46. Department of Public Health, University of Helsinki, Helsinki, Finland.
47. Department of Public Health and Primary Care, Institute of Public Health, University of Cambridge School of Clinical Medicine, Cambridge, UK.
48. Saw Swee Hock School of Public Health, National University Health Systems, National University of Singapore, Singapore, Singapore.
49. Division of Human Genetics, Genome Institute of Singapore, Singapore, Singapore.
50. Department of Ophthalmology and Visual Sciences, University of Utah, Moran Eye Center, Salt Lake City, USA.
51. Ophthalmology and Visual Sciences, University of Wisconsin-Madison, Madison, WI, USA.
52. MRC Social, Genetic and Developmental Psychiatry Centre, Institute of Psychiatry, Psychology & Neuroscience, King's College London, London, UK.
53. Department of Clinical Chemistry, Fimlab laboratories and School of Medicine, University of Tampere, Tampere, Finland.
54. Genetic Epidemiology Laboratory, QIMR Berghofer Medical Research Institute, Herston, Brisbane, Queensland, Australia.
55. Department of Ophthalmology, Yokohama City University School of Medicine, Yokohama, Kanagawa, Japan.
56. Institute of Human Genetics, Technical University Munich, Munich, Germany.
57. Centre for Vision Research, Department of Ophthalmology and Westmead Institute for Medical Research, University of Sydney, Sydney, Australia.
58. Department of Ophthalmology and Visual Sciences, Kyoto University Graduate School of Medicine, Kyoto, Japan.
59. Suraj Eye Institute, Nagpur, Maharashtra, India.
60. Department of Health Sciences and Gerontology Research Center, University of Jyväskylä, Jyväskylä, Finland.

61. Department of Ophthalmology, Central Hospital of Central Finland, Jyväskylä, Finland.
62. Institute of Genetic and Biomedic Research, National Research Council, Cagliari, Italy.
63. Faculty of Medicine, University of Split, Split, Croatia.
64. Institute of Ophthalmology, Moorfields Eye Hospital, London, UK.
65. Research Centre of Applied and Preventive Medicine, University of Turku, Turku, Finland.
66. Department of Clinical Physiology and Nuclear Medicine, Turku University Hospital, Turku, Finland.
67. Gerontology Research Center, University of Jyväskylä, Jyväskylä, Finland.
68. Department of Ophthalmology, University of Pennsylvania, Philadelphia, Pennsylvania, USA.
69. Max Planck Institute for Psycholinguistics, Wundtlaan 1, 6525 XD Nijmegen, The Netherlands.
70. Deptartment of Genetics, Genomics and Informatics, University of Tennessee Health Science Center, Memphis, TN, USA.
71. Department of Medicine, National University of Singapore, Singapore, Singapore.
72. Department of Statistics and Applied Probability, National University of Singapore, Singapore, Singapore.
73. Department of Ophthalmology, Sisters of Mercy University Hospital, Zagreb, Croatia.
74. MRC Epidemiology Unit, Institute of Metabolic Sciences, University of Cambridge, Cambridge, UK.
75. Department of Ophthalmology, Helsinki University Central Hospital, Helsinki, Finland.
76. Department of Epidemiology, Johns Hopkins Bloomberg School of Public Health, Baltimore, Maryland, USA.
77. Wilmer Eye Institute, Johns Hopkins School of Medicine, Baltimore, MD, USA.
78. Centre for Myopia Research, School of Optometry, The Hong Kong Polytechnic University, Hong Kong, Hong Kong.
79. Department of Health Technology and Informatics, The Hong Kong Polytechnic University, Hong Kong, Hong Kong.